N-63-3-1

NOLTR 62-45
REACTORS-GENERAL

A METHOD FOR MEASURING INTERNAL BLAST PRESSURE-TIME HISTORIES OF CONFINED, SODIUM-CASED EXPLOSIONS

9 AUGUST 1962

NOL

UNITED STATES NAVAL ORDNANCE LABORATORY, WHITE OAK, MARYLAND

NOLTR 62-45

NOLTR 62-45

A METHOD FOR MEASURING INTERNAL BLAST PRESSURE-TIME HISTORIES OF CONFINED, SODIUM-CASED EXPLOSIONS

Prepared by:
Harry B. Benefiel

ABSTRACT: Experiments are currently being conducted at the Naval Ordnance Laboratory in an idealized model of the Enrico Fermi Nuclear Reactor for the purpose of determining the response of a model shield plug to simulated excursion-type loadings. These experiments were designed to assess quantitatively the effect that various significant parameters have upon responses of the plug. It is essential that pressure-time histories resulting from the initiation of sodium-cased explosive charges within the piston-fitted model be known, in that the "internal-blast" pressure is the overriding plug-loading consideration.

A pressure-measuring system utilizing a recording oscilloscope and an electro-mechanical, variable-reluctance pressure gage coupled with a fluid-filled, pressure-transmitting tube has been developed and used to measure pressure-time histories for 48 experiments. A method is presented here by which confidence in the validity of the experimental results can be evaluated. Pressure-time data for 21 of these experiments are tabulated and evaluated for validity.

The recorded pressure-time histories and the high-confidence in their validity prove the method to be sound and workable.

Air-Ground Explosions Division
J. F. Moulton, Jr., Chief

PUBLISHED FEBRUARY 1963

EXPLOSIONS RESEARCH DEPARTMENT
U. S. NAVAL ORDNANCE LABORATORY
WHITE OAK, MARYLAND

NOLTR 62-45 9 August 1962

A Method for Measuring Internal Blast Pressure-Time Histories of Confined, Sodium-Cased Explosions

The work of this report was carried out under Task V of Task NOL-285, NOL Reactor-Vessel Containment Program. The objective of Task V is to determine, through experiments in idealized models of the Enrico Fermi Nuclear Reactor, the response of a model shield plug to simulated excursion-type loadings. The report presents internal blast pressure-time histories and the method of measurement for 21 of the experiments performed under Task V. This material was submitted in fulfillment of the thesis requirements for the M.S. degree in Mechanical Engineering at the University of Maryland.

The mention of names of proprietary products in this report constitutes neither an endorsement nor criticism of these products by the United States Government or by the Naval Ordnance Laboratory.

R. E. ODENING
Captain, USN
Commander

C. J. Aronson

C. J. ARONSON
By direction

CONTENTS

ILLUSTRATIONS

TABLES

NOMENCLATURE

A .... frontal area of plug, in^2

a .... cross-sectional area of pressure-transmitting tube sections, in^2

d .... diameter of pressure-transmitting tube sections, in

F .... viscous force of damping fluid, lb

F_t ... total viscous force of damping fluid, lb

F_p ... frictional force of plug, lb

g .... acceleration due to gravity, ft/sec^2

H .... maximum height achieved by plug, ft

h .... degree-of-damping constant for pressure-sensing device

k .... spring constant of pressure-transducer diaphragm, lb/in

L .... length of pressure-transmitting tube sections, in

m_d ... mass of pressure-transducer diaphragm, slugs

m_e ... equivalent mass of damping fluid in pressure-transmitting tube sections, slugs

m_t ... total effective mass of vibrating system (damping fluid in pressure-transmitting tube plus diaphragm) referred to diaphragm, slugs

m_p ... mass of plug, slugs

P .... transient interr.l-blast pressure acting on frontal area of plug, psig

P_i ... peak internal-blast pressure, psig

P_s ... peak shock pressure, psig

PE ... maximum potential energy of plug, ft-lb

r_t ... total damping constant of pressure-sensing device referred to diaphragm, lb-sec/in

r_c ... total critical-damping constant of pressure-sensing device referred to diaphragm, lb-sec/in

s .... displacement of plug, ft

s_f ... displacement of plug at end of power stroke, ft

s_t ... displacement of plug within plug-guide tube, ft

t .... time, sec

u .... average damping fluid velocity in pressure-transmitting tube sections, in/sec

v .... velocity of plug, ft/sec

v_f ... velocity of plug at end of power stroke, ft/sec

x .... displacement of pressure-transducer diaphragm, in

$\frac{dx}{dt}$ ... velocity of pressure-transducer diaphragm, in/sec

$\frac{d^2x}{dt^2}$ .. acceleration of pressure-transducer diaphragm, in/sec^2

μ .... viscosity of damping fluid, lb-sec/in^2

ρ .... mass density of damping fluid, slugs/in^3

INTRODUCTION

This report presents a method by which particularized pressure-time histories were measured for sodium-cased explosions in an idealized scale model of the Enrico Fermi Nuclear Reactor.

The Fermi Reactor Plant is a fast breeder, 100,000-KW facility currently being constructed at Lagoona Beach, Michigan. Figures 1 and 2 show simplified elevation and plan views, respectively, of the reactor plant. A preliminary study, Reference (a), has been made on the capability of the Fermi Plant to contain a nuclear excursion equivalent in violence to the detonation of 1,000 pounds of TNT located at the core of the reactor. Among other results of this study, it was indicated that the 143-ton reactor shield plug would be negligibly sensitive to the shock from a 1,000-lb TNT accident, but that the plug might be significantly responsive to the resulting internal-blast pressure. The internal-blast pressure is defined as the pressure generated within the secondary shield by expanding gases released from the explosive charge. For the reason that internal-blast pressure is dependent upon volume and not configuration, the secondary shield shown in Figures 1 and 2 as an intricate polyhedron can be idealized as a right-circular cylinder of equal volume. In order to assess quantitatively in the laboratory the response of the plug, the idealized reactor model

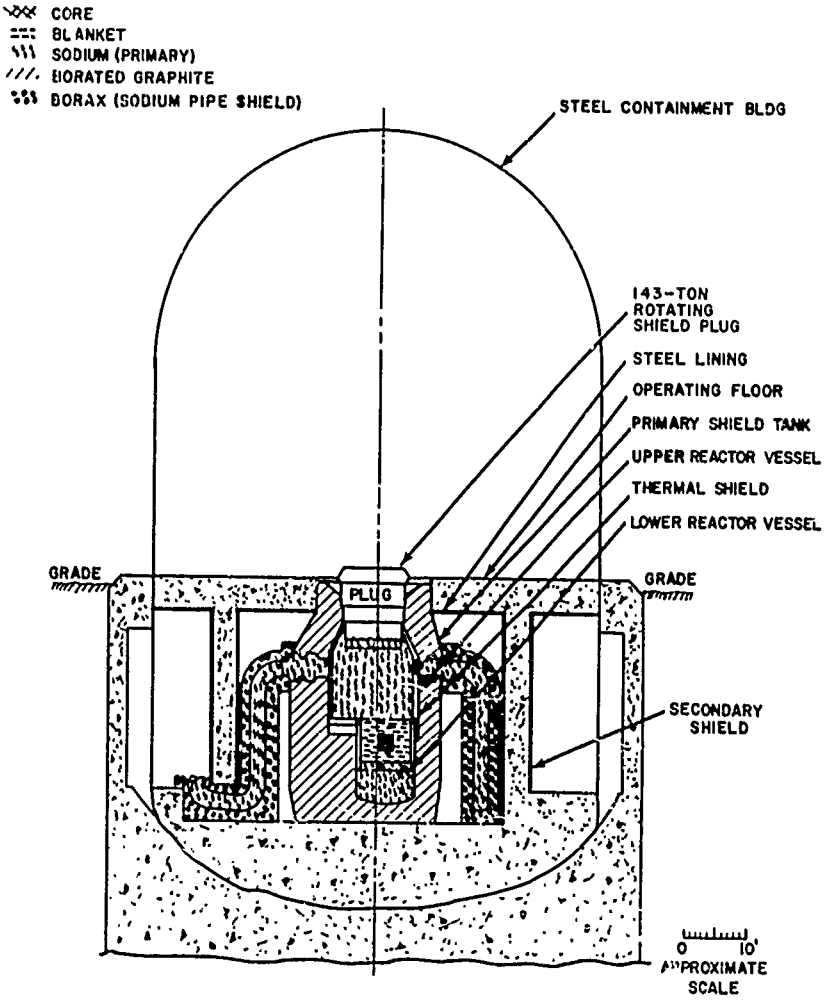

FIG. 1 ELEVATION VIEW OF REACTOR

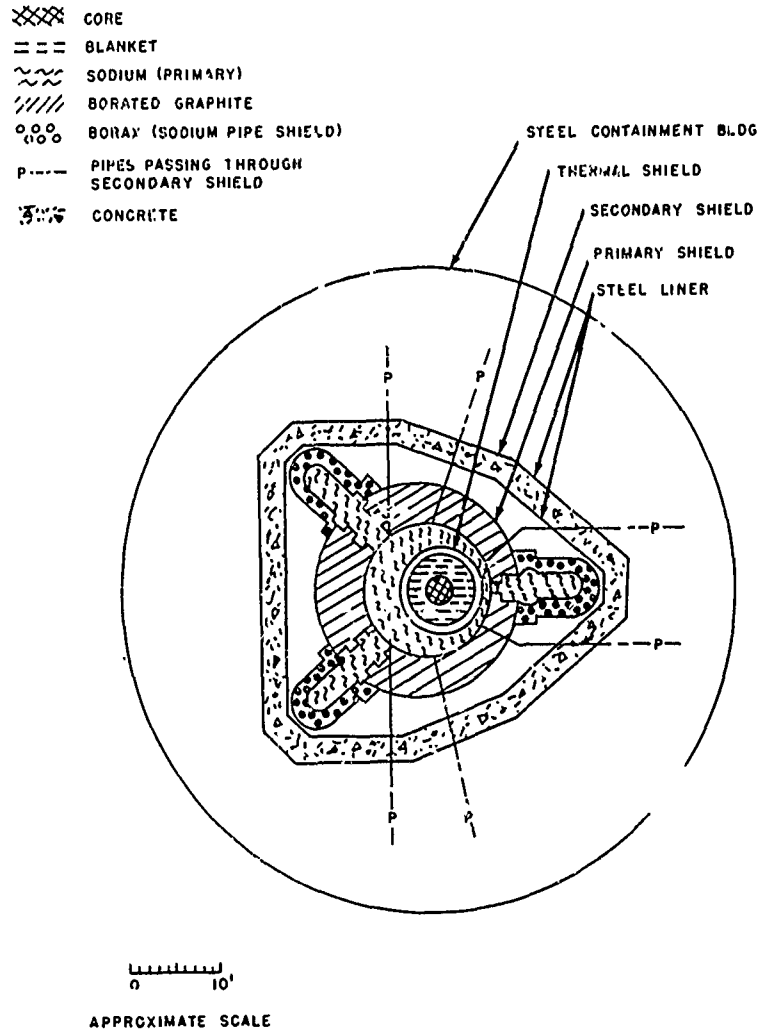

FIG. 2 PLAN VIEW OF REACTOR BELOW OPERATING FLOOR

was scaled by a factor of 1/30, and experiments were conducted in which pentolite charges cased with molten sodium were detonated in the model.

A method for measuring the internal blast pressure-time histories is presented, and this method was used to measure pressure-time histories in a series of tests conducted in an idealized 1/30-scale model reactor. The pressure-time histories for these experiments are given along with a relationship for model plug jump as a function of peak internal-blast pressure.

A procedure is shown and evaluated by which confidence in the validity of the experimental results is strengthened. The high-confidence level of the pressure-time histories obtained from these tests proves the method to be sound and workable.

Ultimately the results obtained from these idealized 1/30-scale model experiments will be utilized in the projection of the plug response from the model to the prototype.

PURPOSE AND OBJECTIVES

The broad purpose of this study was to develop a method for measuring internal blast pressure-time histories generated from the initiation of sodium-cased explosions surrounded by an oxygen-depleted atmosphere and confined within a closed piston-fitted vessel.

The technical objectives were as follows:

1. To develop and design an instrumentation system capable of measuring the internal blast pressure-time histories.

2. To measure the internal blast pressure-time histories in a series of tests conducted in an idealized model of the Enrico Fermi Atomic Power Reactor.

3. To develop a relationship between the peak internal-blast pressure and the maximum height achieved by the plug of the idealized model.

METHOD OF MEASUREMENT

Internal blast pressure-time histories were measured at the Naval Ordnance Laboratory, White Oak, Maryland, in an idealized 1/30-scale model. The basic configuration of the model was that of a closed, piston-fitted, right-circular cylinder, a cross-sectional view of which is shown in Figure 3. The model was divided into three major parts: (1) the secondary shield, (2) the sodium vessel or explosive-charge casing, and (3) the model plug. The secondary shield was a right-circular, steel cylinder with inside diameter and height of 10.0 inches and 9.2 inches, respectively, and it was equipped with a number of access ports that were utilized to control and monitor the various experimental parameters. The sodium vessels were made from 1/32-inch stainless-steel, with a right-cylindrical configuration. The dimensions of the vessels varied and were dictated by the quantity of sodium-casing under investigation. The model plug was a lead-filled, steel piston, 3.5 inches in diameter, 109 inches in length, and 305 pounds in weight, fitted

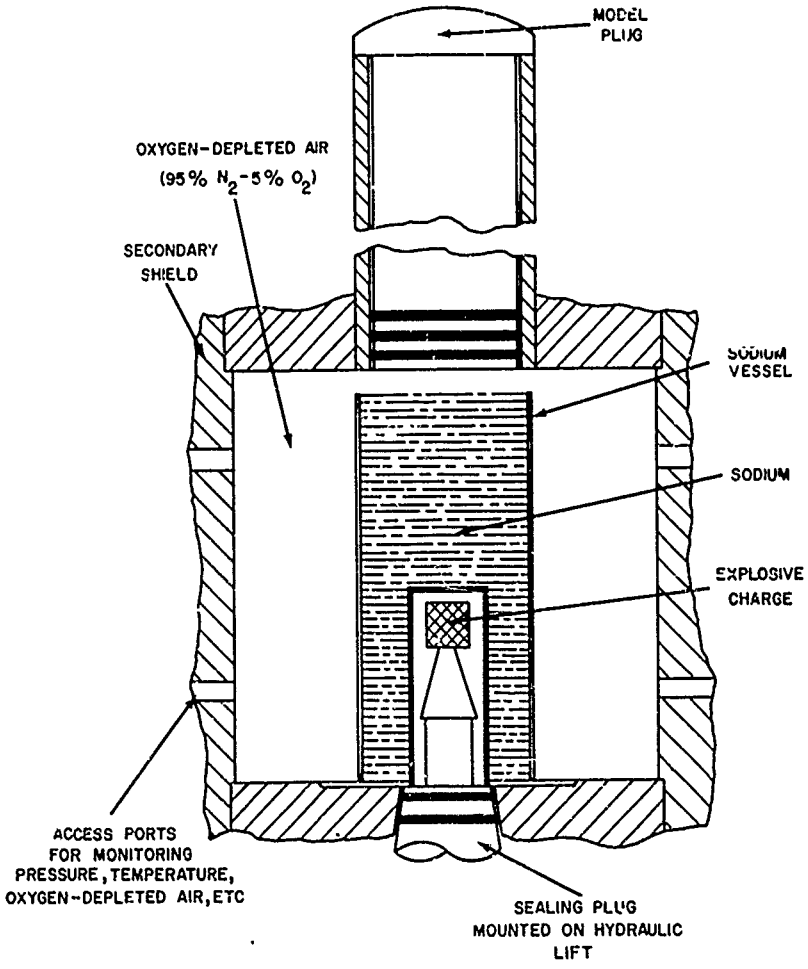

FIG. 3 CROSS-SECTIONAL VIEW OF MODEL REACTOR

with three teflon piston rings on one end. In the experiments the plug was free to slide in a tubular guide that enabled it to travel a pressure-sealed stroke of up to six feet. This pressure-sealed stroke is referred to as the power stroke of the plug. The sodium-cased charges used in the experiments were 15.8 grams of pentolite; these were detonated in the models to examine the effects that significant parameters, such as quality, magnitude, and temperature of the casing, have upon the response of the plug. The initiation of a sodium-cased explosive charge within the model resulted in a complex pressure-time loading function consisting essentially of a sharp-rising shock pulse followed by a slowly decaying internal-blast pressure. The internal-blast-pressure portion of this loading function was measured by means of an instrumentation system consisting basically of a pressure-sensing device and a recorder. The pressure-sensing device was designed so as to damp out the shock pulse, but, nevertheless, to record the internal-blast-pressure portion of the loading function. The theory of viscous damping was employed in designing the instrumentation to fulfill the required damping characteristics.

Requirements. The general configuration of the pressure-time loading function resulting from the initiation of a sodium-cased explosive charge confined within the model is shown in the following diagram.

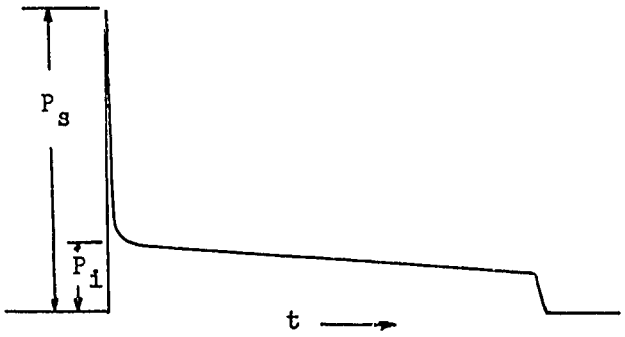

where

P_s ... is peak shock pressure

P_i ... is peak internal-blast pressure

P_s ... is $\approx$ 10 P_i

t ... is time.

Previous investigations, Reference (a), of related shock-wave phenomena have shown that the overriding plug-loading mechanism is the internal-blast pressure, which is defined as the pressure generated within the secondary shield by the expanding gas resulting from detonation of the charge. Since the internal-blast pressure persists for a period of time that is long relative to that of the shock pressure, it is sometimes called the equilibrium pressure. The basis for this may be seen in the above diagram. For the case of the 1/30-scale model, it is that portion of the pressure-time history from approximately one millisecond through the duration of the loading function. Dictated by the parameters and the test conditions of the 1/30-scale model experiments, the

pressure-measuring instrumentation must fulfill the following requirements:

1. the gage must withstand, without damage, shock pulses of the order of 5,000 psi of one-millisecond duration.

2. the entire system must measure and record internal-blast pressures ranging from 5 to 400 psig of 100 to 2,000-milliseconds duration.

3. the gage must operate in a corrosive sodium-contaminated medium.

Instrumentation. Exploratory pressure-time measurements were made utilizing the inductance-gage type, static-pressure measuring instrumentation of W. S. Filler, Reference (b). The exploratory measurements proved the feasibility of attempting to measure the internal blast pressure-time histories; however, owing to the unsuitability of this equipment for use in a sodium-contaminated medium, the following system was developed.

The system consists basically of a pressure-sensing device and a recorder, the pressure-sensing device being a DCS-4 pressure gage coupled to a pressure-transmitting tube. The DCS-4 pressure gage, manufactured by Consolidated Controls Corporation, Albuquerque, New Mexico, is a voltage-regulated gage that combines an S-80 variable-reluctance, diaphragm-type pressure transducer with stable transistorized electronic circuitry. The DCS-4 gage, an exploded view of the S-80 transducer, and a detailed schematic of the electronic circuitry are shown respectively in Figures 4, 5, and 6. The DCS-4 gage is operated from a 23-volt D. C.

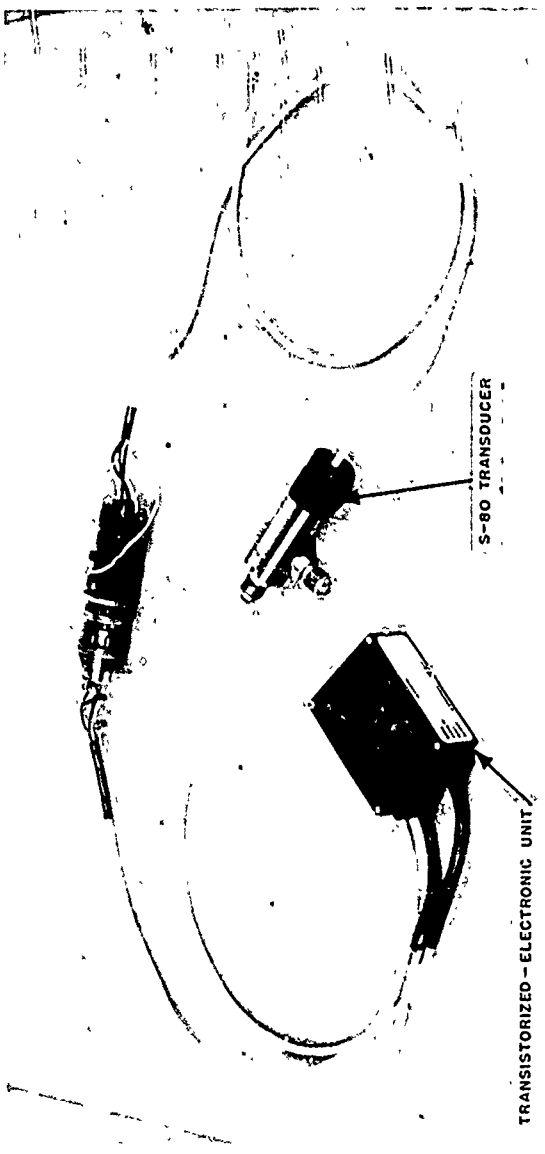

FIG. 4 DCS-4 PRESSURE GAGE

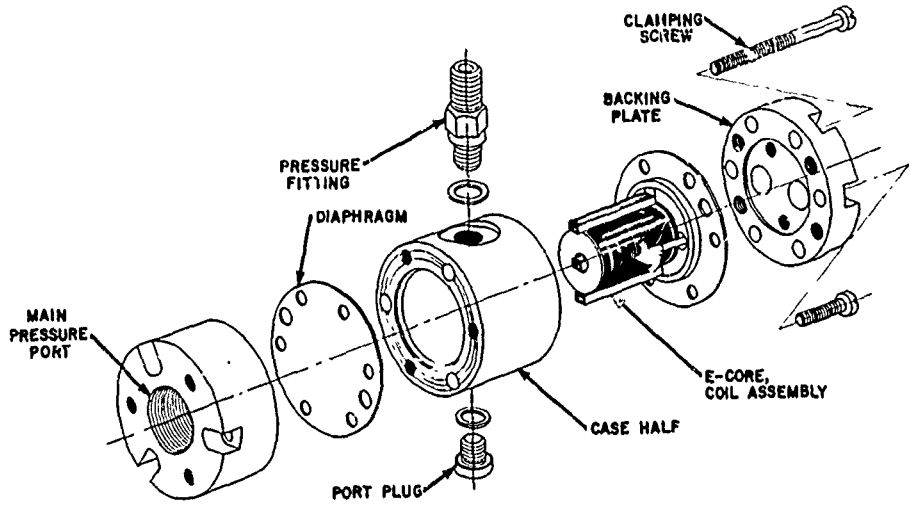

FIG. 5 EXPLODED VIEW OF PRESSURE TRANSDUCER

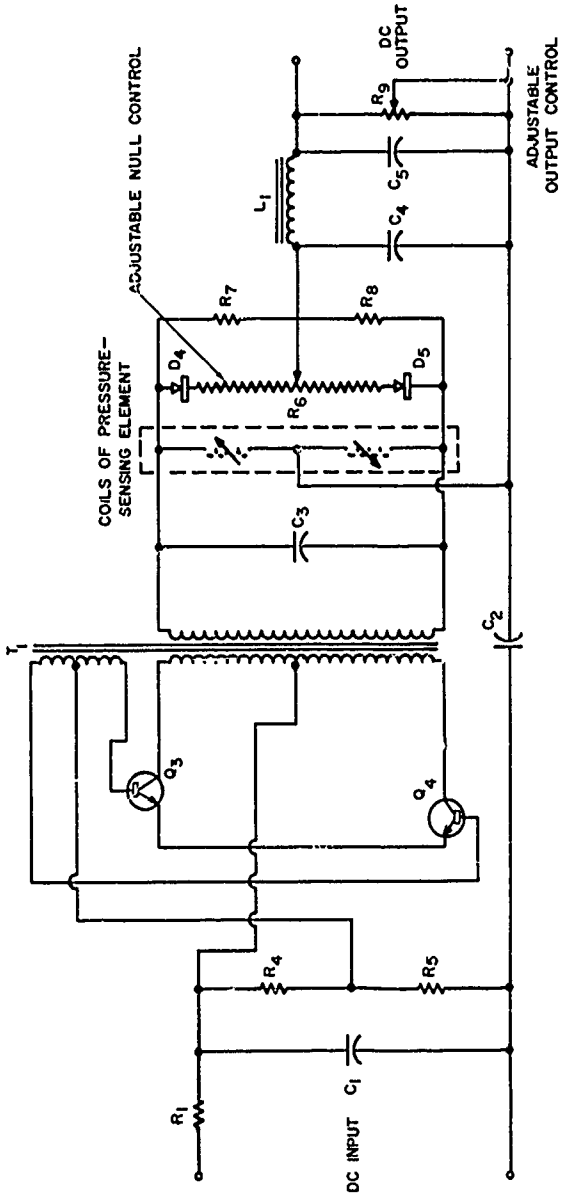

FIG.6 SCHEMATIC DIAGRAM OF PRESSURE GAGE

power supply and has a signal output of 0-3 volts D. C. over the rated pressure range of the transducer. The signal output is proportional to the pressure signal applied to the transducer. In order to measure the internal-blast pressure with a good degree of accuracy, the range of the pressure transducer must be compatible with the magnitude of the internal-blast pressure.

To prevent the pressure transducer from being damaged by the shock pulse, a pressure-transmitting tube was placed between the transducer and the pressure source. The transmitting tube was made of steel, and its dimensions were controlled by the degree of damping desired. Through evolution of the pressure-measuring system, two types of transmitting tubes were developed, an orifice-damping type and a fluid-damping type. A cross-sectional view of the two types is shown in Figure 7. The orifice-type transmitting tube, evolved first, used air as its pressure-transmitting medium and an orifice as its damping control (the smaller the diameter of the orifice plug, the greater the damping). This type of transmitting tube was used successfully in those tests where sodium was not present in the explosive-charge casing. However, in the tests where sodium was present, clogging occurred in the orifice-type transmitting tube and prevented the complete measurement of the pressure-time history. This clogging resulted from particles of liquid sodium being forced into the air-filled transmitting tube and subsequently solidifying. To prevent this, the orifice plug was removed, and the tube was filled with a

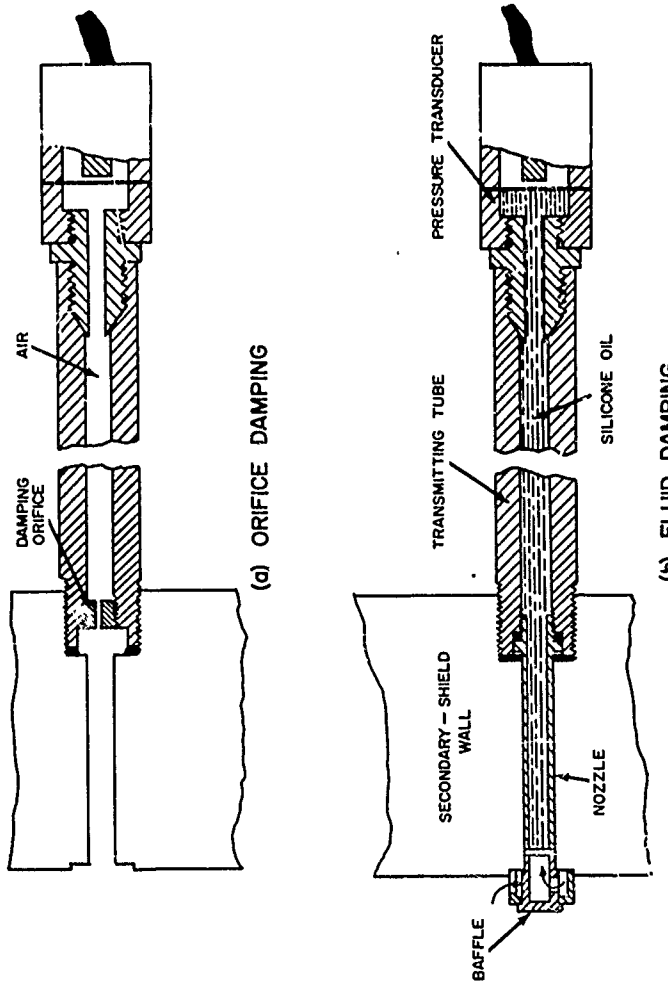

FIG. 7 CROSS – SECTIONAL VIEW OF PRESSURE – SENSING DEVICE INSTALLED IN SECONDARY – SHIELD WALL

viscous fluid (oil), resulting in the second type transmitting tube. A nozzle was attached to the tube to extend the fluid medium to the inside of the secondary-shield wall. A labyrinth-type baffle was inserted into the inside wall opening of the pressure-measuring port in order to reduce the velocity of the liquid sodium and other foreign matter impinging on the fluid column. The degree of damping was controlled by varying the dimensions of the tube and the viscosity and density of the pressure-transmitting fluid. A detailed presentation of damping is treated in the section on damping theory. The recorder used in the pressure-measuring instrumentation was a Tektronix Oscilloscope equipped with a Polaroid Land Camera. A view of the recording system is shown in Figure 8. The oscilloscope recorded the D.C. voltage-time history received from the DCS-4 pressure gage; and by means of a static-calibration curve of the pressure gage, this voltage-time trace was transposed to a pressure-time curve. Type 46-L Land film was used in the Polaroid Land Camera because it produces a positive transparency, enabling the data to be reduced and analyzed directly on a film reader.

To gain reliability, two independent pressure sensing systems were used in conjunction with two Tektronix Oscilloscopes. The signals from both DCS-4 pressure gages were recorded on each oscilloscope, equipped with a type 53C Dual-Trace Plug-in Preamplifier Unit. By using the chopper circuit of the plug-in unit, pressure signals from both pressure gages were displayed

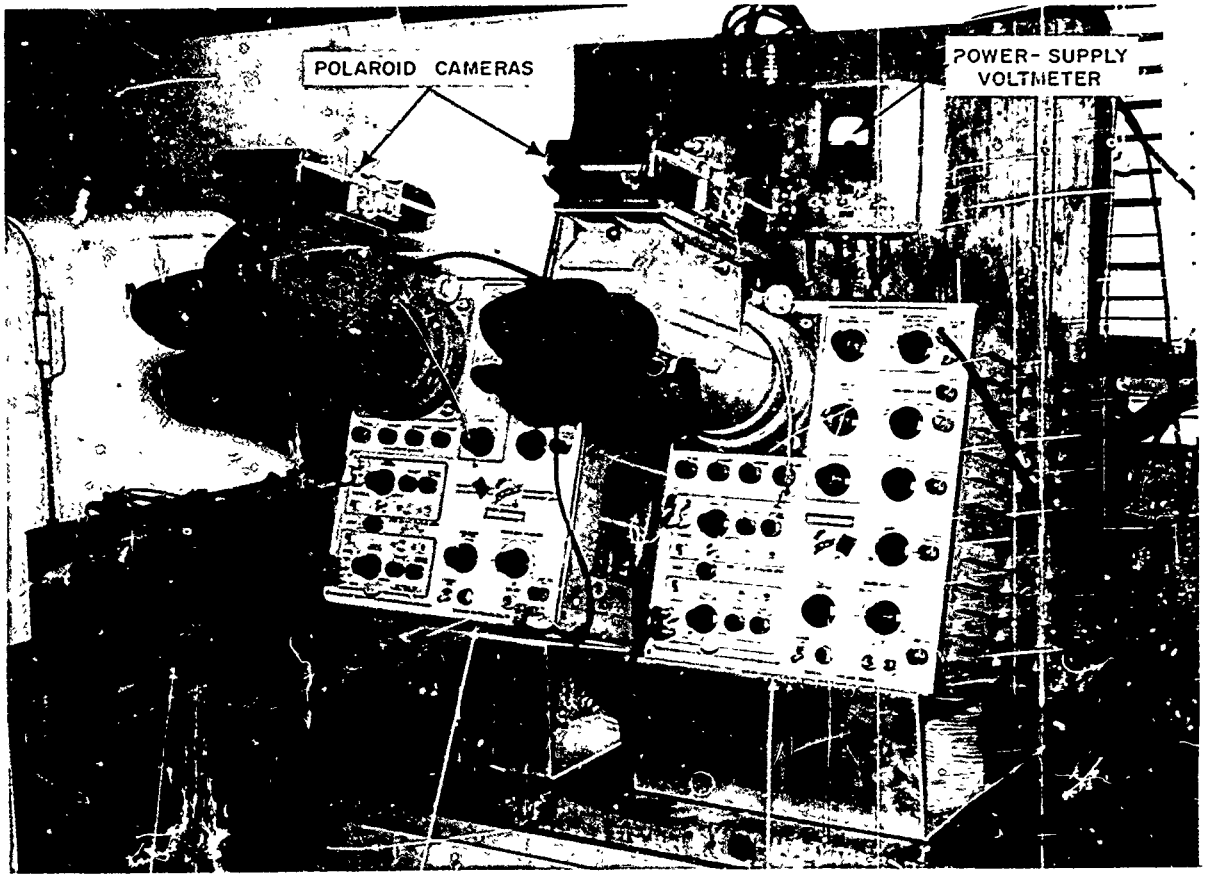

FIG. 8 RECORDING OSCILLOSCOPES

simultaneously on each oscilloscope. In view of the various horizontal-beam sweep rates available in the oscilloscope, the sweep rate of one oscilloscope was set to display the early portion of the pressure-time history, and the second oscilloscope was set to display the pressure-time history throughout the complete power stroke of the model plug. A line diagram of the pressure-measuring system is shown in Figure 9. Oscilloscope traces for test No. 25, shown in Figure 10, are similar to the pressure loading function shown in page 8. However, owing to the damping characteristics of the pressure-measuring system, the sharp-rising shock pulse does not appear on the oscilloscope traces.

Damping Theory. As previously stated, damping in the transmitting tube can be controlled by varying the dimensions of the tube and the viscosity and density of the transmitting fluid. This can be shown analytically by invoking the theories of vibration and viscous flow. Consider the pressure transducer coupled with the transmitting tube to be filled with a fluid of density, ρ, and viscosity, μ, and represented by the schematic diagram shown on page 20:

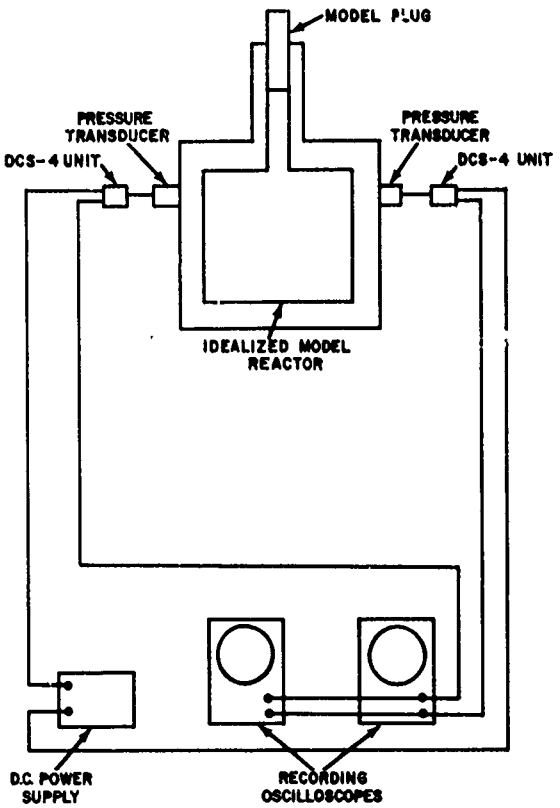

FIG. 9 LINE DIAGRAM OF PRESSURE-MEASURING SYSTEM

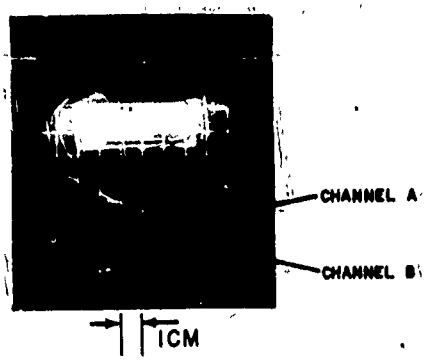

OSCILLOSCOPE NO.1
TIME: 100 MSEC/CM

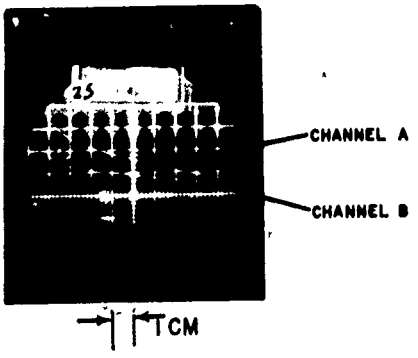

OSCILLOSCOPE NO.2.
TIME: 20 MSEC/CM

FIG. 10 PRESSURE-TIME OSCILLOSCOPE TRACES OF TEST NO. 25

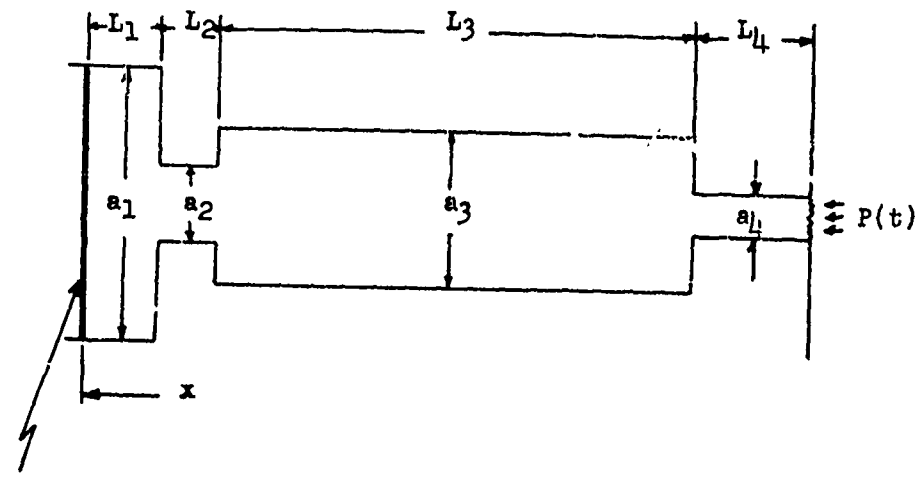

where the nomenclature is

a .... cross-sectional area of tube sections, in^2

d .... diameter of tube sections, in

F .... viscous force of fluid, lb

F_t ... total viscous force of fluid referred to diaphragm, lb

h .... degree-of-damping constant

k .... spring constant of diaphragm, lb/in

L .... length of various tube sections, in

m_d ... mass of diaphragm, slugs

m_e ... equivalent mass of fluid in tube sections referred to diaphragm, slugs

m_t ... total effective mass of vibrating system (damping fluid in tubes plus diaphragm) referred to diaphragm, slugs

r_o ... total critical-damping constant referred to diaphragm, lb-sec/in

r_t ... total damping constant referred to diaphragm, lb-sec/in

t .... time, sec

u .... average fluid velocity in tube sections, in/sec

x .... displacement of diaphragm, in

$\frac{dx}{dt}$ ... velocity of diaphragm, in/sec

$\frac{d^2x}{dt^2}$ .. acceleration of diaphragm, in/sec^2

μ .... viscosity of fluid, lb-sec/in^2

ρ .... mass density of fluid, slugs/in^3

subscripts

1 .... pressure-transducer section

2 .... pressure-transducer adapter section

3 .... transmitting-tube main section

4 .... transmitting-tube nozzle section.

Pressure P(t) acts upon the nozzle of the transmitting tube, and if the fluid is taken to be incompressible and to move as a unit, the diaphragm deflects a distance, x. The motion of the fluid can be considered analogous to that of a spring-mass system, the free-body diagram of which is shown on page 22.

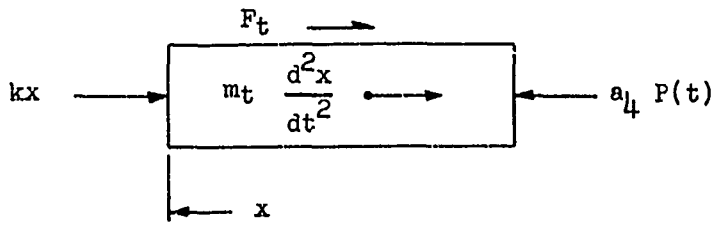

If losses due to the varying cross-sections are neglected, the equilibrium equation for the fluid mass referred to the diaphragm is

$$m_t \frac{d^2x}{dt^2} + F_t + kx = a_4 P(t) \qquad (1)$$

Since flow in the transmitting tube is laminar at the low Reynolds' number ordinarily encountered, the expression for the viscous force can be derived from the theory of laminar viscous flow for incompressible fluids in circular tubes and is

$$F = 8\pi\mu L u \qquad (2)$$

The total viscous force, F_t, can be expressed as the sum of the viscous forces of each section and is

$$F_t = F_1 + F_2 + F_3 + F_4 \qquad (3)$$

Substituting the expression for F from equation (2) for each section in the above equation, we obtain

$$F_t = 8\pi\mu L_1 \frac{dx}{dt} + 8\pi\mu L_2 u_2 + 8\pi\mu L_3 u_3 + 8\pi\mu L_4 u_4 \qquad (4)$$

From the principle of conservation of mass, we obtain the following relationships

$$u_2 = \frac{a_1}{a_2}\frac{dx}{dt}; \quad u_3 = \frac{a_1}{a_3}\frac{dx}{dt}; \quad u_4 = \frac{a_1}{a_4}\frac{dx}{dt} \qquad (5)$$

and substituting these relationships into equation (4) and combining terms, we obtain F_t referred to the diaphragm to be

$$F_t = 8\pi\mu\left[L_1 + \frac{a_1}{a_2} L_2 + \frac{a_1}{a_3} L_3 + \frac{a_1}{a_4} L_4\right]\frac{dx}{dt} \qquad (6)$$

Letting

$$r_t = 8\pi\mu\left[L_1 + \frac{a_1}{a_2} L_2 + \frac{a_1}{a_3} L_3 + \frac{a_1}{a_4} L_4\right]$$

and substituting the expression for F_t from the above equation in equation (1), we obtain

$$m_t \frac{d^2x}{dt^2} + r_t \frac{dx}{dt} + kx = a_4 P(t) \qquad (7)$$

the solution of which, for the case of vibrating motion, is

$$x = e^{-\frac{r_t t}{2m_t}}\left[A \cos\sqrt{\frac{k}{m_t} - \left(\frac{r_t}{2m_t}\right)^2}\, t + B \sin\sqrt{\frac{k}{m_t} - \left(\frac{r_t}{2m_t}\right)^2}\, t\right] + Y_p \quad (8)$$

where Y_p represents the particular integral for pressure, P(t). The degree of damping, h, of the vibrating system is expressed as the ratio

$$h = \frac{r_t}{r_o} \quad (9)$$

where r_o is the critical damping constant given by

$$r_o = 2\sqrt{k\, m_t} \quad (10)$$

In determining the total effective mass (m_t) of the fluid referred to the diaphragm, we must give consideration to the fact that the velocity distribution in the various sections is not uniform but is represented by a paraboloid of revolution. Because of this fact, the mass of the fluid in each section is referred to as an equivalent mass, m_e, with an average velocity, u. This equivalent mass is equal to 4/3 the actual mass, Reference (c); it can be expressed as

$$m_e = 4/3\ \rho\ a\ L \quad (11)$$

and when referred to the diaphragm is defined as

$$m_e = 4/3\ \rho\ a\ L \left[\frac{a_1}{a}\right]^2 \qquad (12)$$

The total effective mass of the system referred to the diaphragm can be expressed as the sum of the equivalent masses of each section referred to the diaphragm plus the mass of the diaphragm and is

$$m_t = m_d + m_{e1} + m_{e2} + m_{e3} + m_{e4} \qquad (13)$$

Substituting in the above equation the relationships obtained from equation (12) for each section and combining terms, we obtain

$$m_t = m_d + 4/3\,\rho \left\{a_1\ L_1 + a_2\ L_2\left[\frac{a_1}{a_2}\right]^2 + a_3\ L_3\left[\frac{a_1}{a_3}\right]^2 + a_4\ L_4\left[\frac{a_1}{a_4}\right]^2\right\} \qquad (14)$$

Thus the expression for the degree of damping becomes

$$h = \frac{4\pi\mu\left[L_1 + \frac{a_1}{a_2}\ L_2 + \frac{a_1}{a_3}\ L_3 + \frac{a_1}{a_4}\ L_4\right]}{\sqrt{k\left\{m_d + 4/3\,\rho\left[a_1\ L_1 + a_2\ L_2\left(\frac{a_1}{a_2}\right)^2 + a_3\ L_3\left(\frac{a_1}{a_3}\right)^2 + a_4\ L_4\left(\frac{a_1}{a_4}\right)^2\right]\right\}}} \qquad (15)$$

The value for the spring constant of the diaphragm, k, can be determined from the load deflection relationship for a uniformly loaded circular plate with clamped edges and a large deflection. A discussion of this is covered in Appendix A.

Equation (15) shows that for a given pressure transducer the degree of damping of the pressure-transmitting tube is a function of the lengths and area ratios of the various sections that make up the tube and the density and viscosity of the fluid within it. Owing to design considerations for the access ports in the secondary-shield wall and the pressure transducer, the number of variables that influence the damping characteristics of the pressure-transmitting tube is greatly reduced. For example, the dimensions of section 4, the nozzle section, are controlled by the size of the access ports; and the dimensions of sections 1 and 2, the cavity and adapter sections of the pressure transducer, are controlled by the design of the transducer. The damping characteristic of the transmitting tube is, therefore, a function only of the length and diameter of the main section and the density and viscosity of the fluid. In order to damp out the shock pulse, the response of the pressure-sensing device can not be faster than one millisecond. Dynamic calibration experiments were conducted to verify the damping theory and to determine the proper fluid and the correct transmitting-tube dimensions to produce the desired response time for the pressure-

sensing device. A detailed discussion of these experiments and the results obtained therefrom is presented in Appendix A.

EXPERIMENTAL FACILITIES

In order to ascertain in the laboratory the response of the shield plug in the Enrico Fermi Atomic Power Plant to an accidental nuclear excursion, it was necessary to conduct experiments in an idealized model. The basic configuration of this model was that of a closed, piston-fitted, right-circular cylinder, a description of which has been presented in the Method of Measurement section. A cross-sectional view of the model is shown in Figure 3. Experiments in this model were conducted to assess quantitatively the parameters that significantly affect the internal-blast pressure function and the resultant plug jump. Only those facilities pertaining to measurement of internal blast pressure-time histories are presented here.

The variable-reluctance pressure transducers coupled with pressure-transmitting tubes were inserted securely into the secondary-shield-wall-access ports of the model. A cross-sectional view of the pressure-sensing device is shown in Figure 7. Signal leads attached to the two pressure transducers were directed to their respective DCS-4 electronic units mounted on the inside wall of the movable platform. From the platform they were directed to the recording oscilloscopes located in the instrumentation and

control building. A view of the recording oscilloscopes is shown in Figure 8. To ensure that the pressure transducers remained at ambient temperature, cooling air from centrifugal blowers mounted on the model adjacent to the transducers was directed on them throughout the test.

In establishing confidence in the validity of the pressure-time data, the dynamics of the model plug were used in concert with the pressure-time data. To correlate the respective histories of the plug displacement and the internal-blast pressure, the motion of the plug had to be monitored. This was achieved by the use of two camera systems, one system using a 16-millimeter Fairchild High-Speed Camera and the second system using a 35-millimeter Mitchell Camera. The Fairchild High-Speed Camera was operated at approximately 1,600 frames per second and was located in the plane of the trajectory, 30 feet directly behind the model on a 30-foot tower. A timing-pulse generator, which was synchronized with a 400-cycles-per-second, vacuum-tube controlled fork, supplied timing pulses to the high-speed camera. The primary purpose of the high-speed camera was to record the displacement-time history of the plug during the power stroke. The 35-millimeter Mitchell Camera was operated at approximately 64 frames per second and was located on a 50-foot tower situated 132 feet from the model along a path at right angles to the flight path of the plug. Its primary purpose was to record the maximum height the

plug achieved. A layout of the camera instrumentation is shown in Figure 11. In order to synchronize the triggering of the recording oscilloscopes and the running of the Fairchild High-Speed and Mitchell cameras with the firing of the explosive charge, a delay-sequence firing unit was used. This unit delayed the delivery of the firing pulse to the explosive charge until the cameras had been started and brought up to speed and the triggering pulses had been delivered to the recording oscilloscopes. The delay time was measured and recorded by oscilloscope No. 3. A block diagram of the electronic instrumentation system is shown in Figure 12.

To ensure that the pressure gages were not damaged during the tests and their calibration altered, each gage was statically calibrated before and after each test with a Type-1300 Ashcroft Dead-Weight Gage Tester. Figure 13 shows a pressure gage being calibrated. In order to achieve the desired damping characteristic required of the pressure-measuring instrumentation, the pressure gages were also calibrated under dynamic conditions. Transient step-pressure pulses from 0 to 500 psi and of the order of 500-microseconds rise time were generated in a pressure pot. The pressure pot consists essentially of two chambers, a reference chamber and a gage chamber, separated by a sealing valve. The volume of the reference chamber is very large relative to that of the gage chamber. The reference chamber was filled to the desired

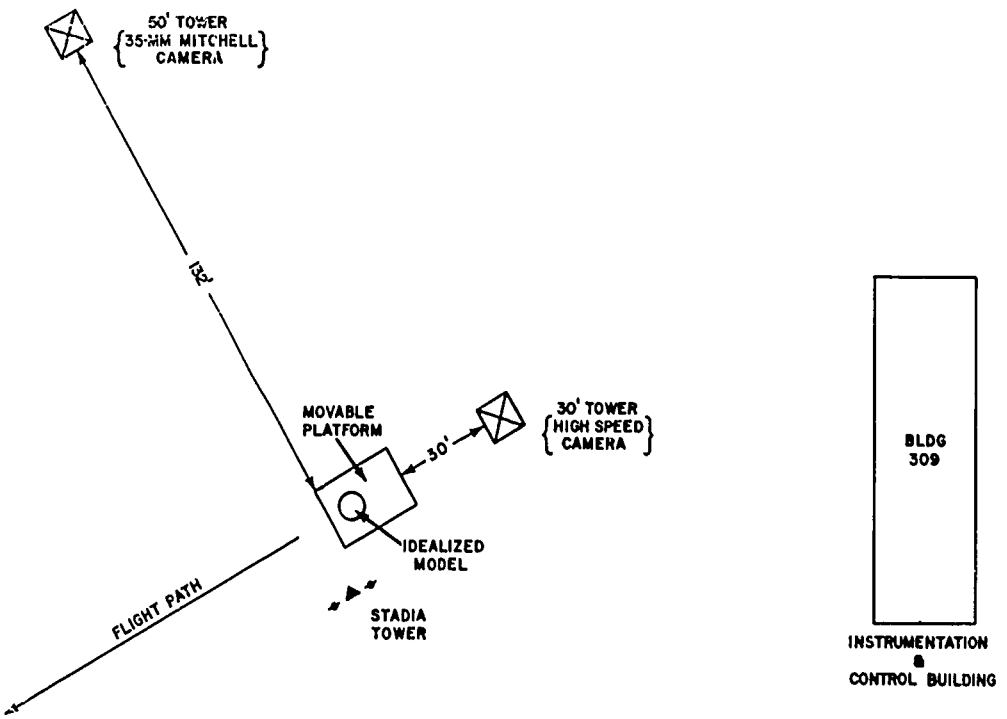

FIG. 11 LAYOUT OF PHOTOGRAPHIC INSTRUMENTATION

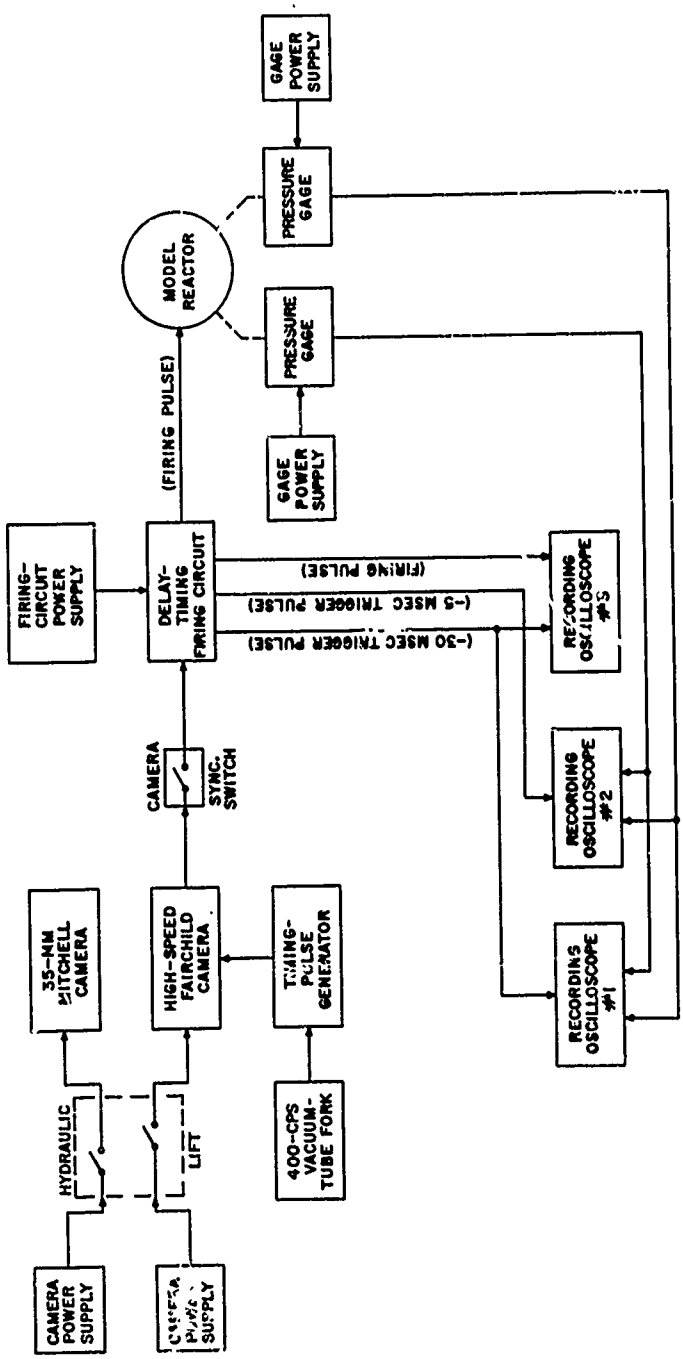

FIG. 12 BLOCK DIAGRAM OF ELECTRONIC INSTRUMENTATION SYSTEM

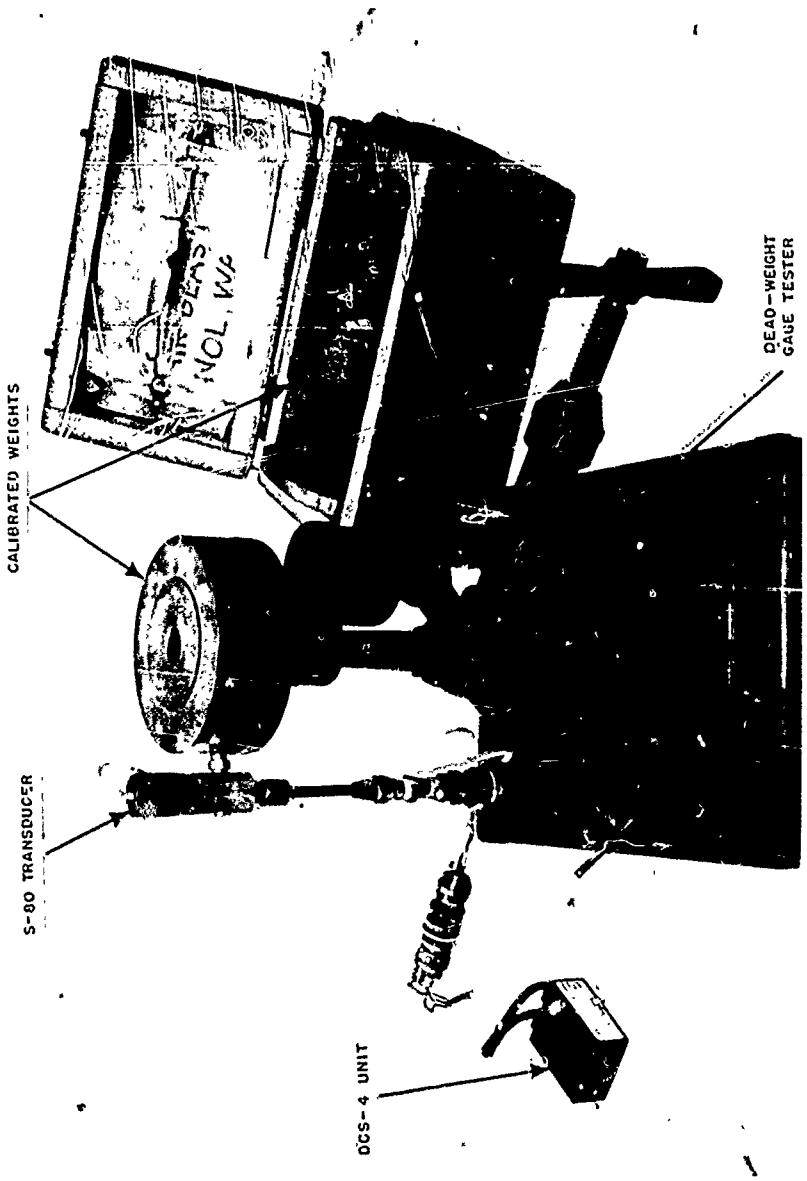

FIG. 13 STATIC CALIBRATION SETUP

pressure with compressed air, and by means of a spring loaded mass, the sealing valve was abruptly released, subjecting the pressure gage in the gage chamber to a sharp-rising pressure pulse. Figure 14 shows a cross-sectional view of the pressure pot. A discussion of the dynamic-calibration experiments is presented in Appendix A.

EXPERIMENTAL PROCEDURES AND RESULTS

Forty-eight experiments in the idealized, 1/30-scale model reactor were conducted to assess quantitatively the parameters that significantly affect the internal-blast pressure loading function and hence the height achieved by the model plug. The principal parameters studied were the quality, magnitude, and temperature of the explosive-charge casing. The internal blast pressure-time histories were measured for all 48 experiments. Some of the experiments were conducted in order to check instrumentation, experimental techniques and procedures, and replicability of the experimental results. Taking these factors into consideration and minimizing redundancy, we elect to present the results of only 21 of the 48 experiments. The selection of these 21 experiments was based upon the objective of illustrating the effects that the principal parameters had upon the internal blast pressure-time histories.

Exploratory experiments were conducted using the pressure pot to dynamically calibrate the pressure-sensing device. The purpose

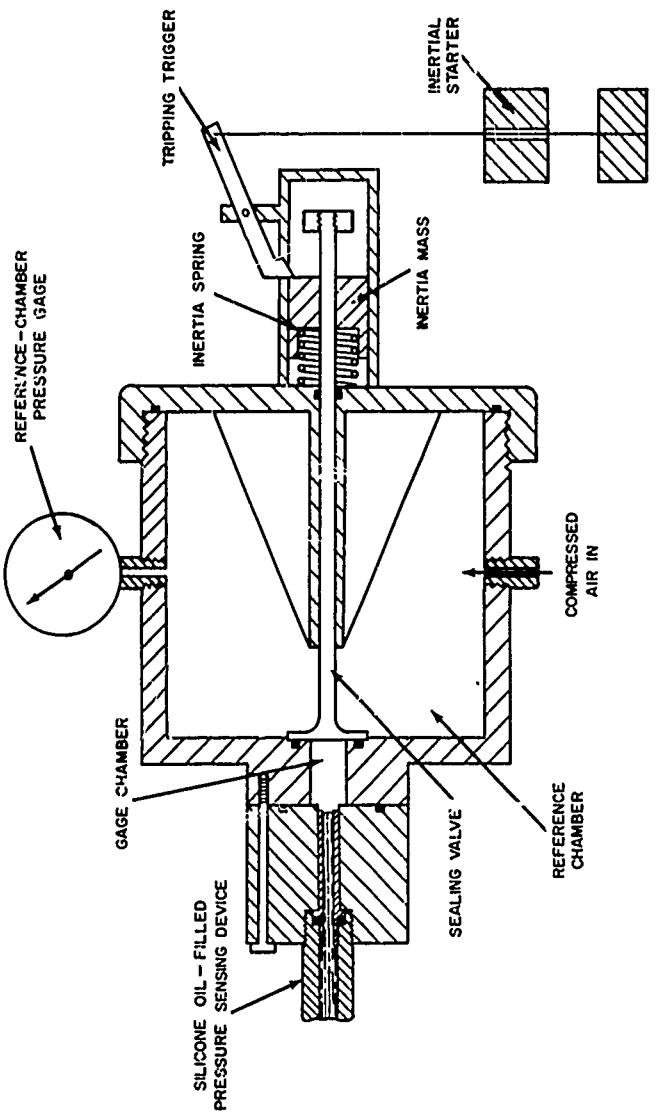

FIG.14 CROSS-SECTIONAL VIEW OF PRESSURE POT

of these experiments was three fold: (1) to determine the dimensions of and the fluid viscosity within the pressure-transmitting tube necessary to produce the required damping, (2) to check out the complete pressure-measuring instrumentation prior to use in the model reactor experiments, and (3) to verify the damping theory. A detailed discussion of these experiments and the results obtained therefrom are presented in Appendix A.

In order to assess how the quality, magnitude, and temperature of the explosive-charge casing affect the internal-blast pressure loading function, experiments were conducted in which various amounts of sodium casings at temperatures of 550 degrees F and 850 degrees F were used. Five different size sodium vessels were used and are referred to in Table 1 as 4*, 8*, 12*, 16*, and 20* (increasing in volume) vessels. A chronological description of the procedure used in measuring the internal blast pressure-time history in these experiments is as follows. Prior to inserting the pressure-transmitting tube into the access ports of the secondary-shield wall of the model, the pressure gages were statically calibrated, as shown in Figure 13. Following static calibration, the transmitting tubes were connected to the pressure transducers and were filled, under vacuum, with type "200" Dow Corning Corporation silicone fluid. The transmitting tubes were then inserted into the access ports of the secondary-shield wall, and the signal leads of the pressure transducer were connected to their respective DCS-4

electronic units located on the inside wall of the movable platform. The centrifugal blowers were turned on to cool the transducers, and then the signal cables from the DCS-4 units to the instrumentation building were connected to recording oscilloscopes No. 1 and No. 2. Just prior to the firing of the explosive charge, the oscilloscopes were adjusted, and when all test conditions were fulfilled the hydraulic lift was raised. The hydraulic lift was used to remotely insert the explosive charge into the liquid-sodium casing. As the hydraulic lift reached certain positions along its travel, microswitches were closed, starting the Mitchell and High-Speed Fairchild cameras in that respective sequence. When the high-speed camera reached its proper speed, the camera sync-switch closed and activated the delay-sequence firing circuit which in turn instantaneously triggered recording oscilloscopes No. 1 and No. 3. At approximately 25 and 30 milliseconds following the triggering of oscilloscopes No. 1 and No. 3, the delay-sequence firing circuit triggered oscilloscope No. 2 and simultaneously delivered a firing pulse to the explosive charge and oscilloscope No. 3, respectively. Subsequent to the closing of the camera microswitches but prior to the detonation of the explosive charge, the hydraulic lift sealed the model reactor and positioned the charge within the casing.

The peak internal-blast pressure, duration of the power stroke of the plug, and maximum height achieved by the plug for

the 21 tests are tabulated in Table 1. The orifice-type pressure-transmitting tube was used in all tests where the explosive-charge casing contained no sodium. In those tests where the explosive-charge casing contained sodium, the fluid-type transmitting tube was used. In several of the non-sodium casing tests, both types of transmitting tubes were used, the orifice-type in one recording channel and the fluid-type in the second recording channel. The purpose of this was to compare under identical test conditions the pressure-time histories measured using each type. No differences between the pressure-time histories were experienced in these tests. Although the response of the fluid-type transmitting tube, as determined by the pressure pot, was such that it should not have transmitted an explosive-shock pulse, in several of the sodium-casing tests, shock pulses appeared in the early portions of the pressure-time records. In all tests where these shocks occurred, a shift in the static-calibration curves resulted, and in a few tests the pressure transducers were permanently damaged. In order to combat this, pressure transducers of much higher ranges than the maximum internal-blast pressure anticipated were used (e.g., 0-300 and 0-500 psi range transducers were used to measure internal-blast pressures of the order of 50 psig) which resulted in a reduction of the sensitivity of the pressure-measuring system. It was later discovered that these shock pulses were caused by particles of liquid sodium and foreign matter

TEST NO.	TEST CONDITIONS				RESULTS		
	TYPE OF ATMOS.	SODIUM CASING WT.	VESSEL TYPE	CASING TEMP.	PEAK PRESSURE	POWER-STROKE DURATION	MAXIMUM PLUG JUMP
	(% O_2)	(GRAMS)		(^oF)	(PSIG)	(MSEC)	(FT)
2	5.6	0	NONE	—	192	354	15.96
29	5.0	0	NONE	—	194	350	15.75
35	4.7	0	NONE	—	185	358	15.62
23	5.5	0	4*	850	112	525	9.48
25	4.5	0	8*	550	110	633	7.29
24	4.5	0	8*	850	108	617	7.73
30	4.3	0	12*	550	160	412	12.51
31	4.3	0	16*	550	137	450	11.61
21	6.0	0	16*	850	96	641	7.58
36	4.9	382	4*	550	66	1016	4.71
37	5.0	382	4*	850	88	601	8.31
38	4.5	732	8*	550	MALFUNCTIONED PRESSURE GAGE		
39	5.0	732	8*	850	72	832	6.56
40	5.0	1162	12*	550	MALFUNCTIONED PRESSURE GAGE		
42	5.0	1162	12*	850	64	966	4.64
43	5.1	1340	16*	550	45	**	3.39
41	5.0	1340	16*	850	66	835	6.52
44	5.4	1747	20*	550	46	870	2.30
45	5.1	1611	20*	850	MALFUNCTIONED PRESSURE GAGE		
47	5.2	1611	20*	850	57	766	2.07
48	5.2	1162	12*	550	54	966	2.50

** Recorder failed to record complete pressure-time history

TABLE I EXPERIMENTAL RESULTS

impinging at high velocities upon the fluid column in the transmitting tube. A labyrinth-type baffle was designed and placed on the inside of the secondary-shield wall in the opening of the access ports in order to reduce the velocities of these impinging particles. Figure 7 shows the position of the baffle plate relative to the transmitting tube. Baffle plates were used in tests No. 47 and 48, and no shock pulses or shifts in the static calibration curves were experienced. The results of tests No. 2, 29, and 35 illustrate the replicability of the pressure-measuring system. The power stroke-time and pressure-time plots for the 21 tests are shown in Figures 15, 16, and 17. The relationship between peak internal-blast pressure and maximum height achieved by the plug is presented graphically in Figure 18.

The internal blast pressure-time traces, shown in Figures 15, 16, and 17, were recorded by the oscilloscopes as voltage-time traces, where voltage is proportional to pressure. The proportionality of pressure to voltage was determined from static-calibration records. Type 46-L Polaroid Land Film, used to record the voltage-time traces and static-calibration data, produced a positive transparency that was easily read and analyzed on a high-magnification Telereadex 29A film reader. The pressure-time curves shown in Figures 15, 16, and 17 were obtained by combining the data from the voltage-time traces with

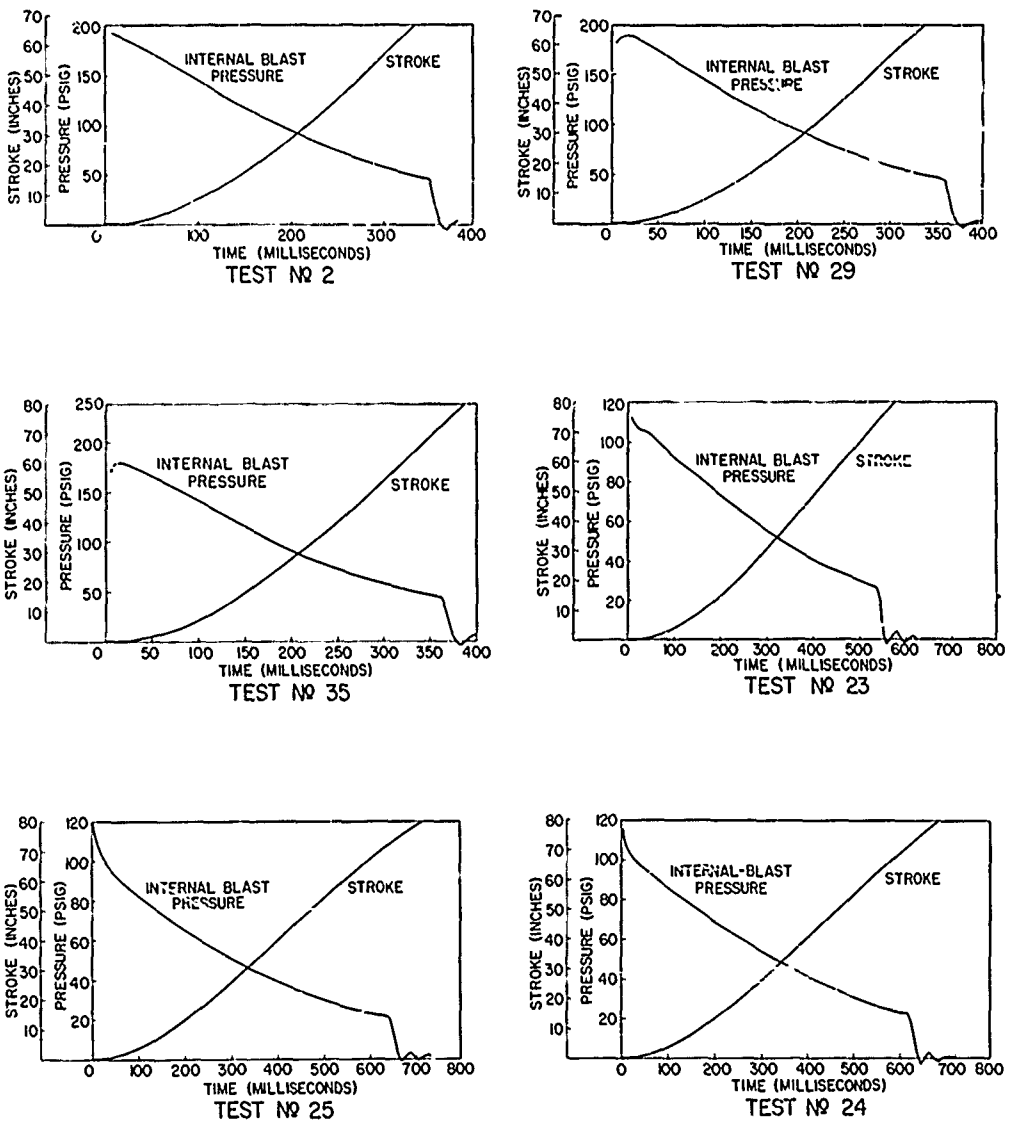

FIG. 15 STROKE-TIME & PRESSURE-TIME PLOTS
FOR TESTS NO. 2, 29, 35, 23, 25, AND 24

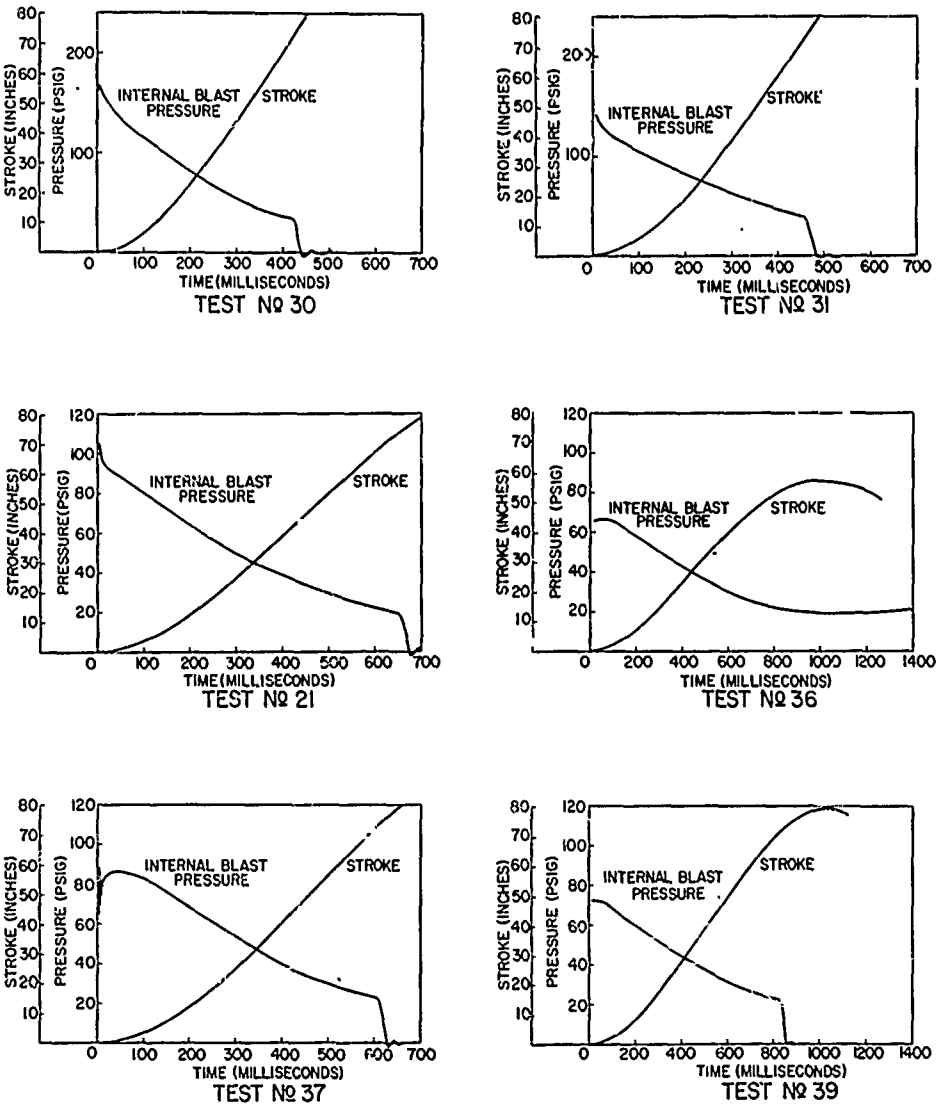

FIG. 16 STROKE-TIME & PRESSURE-TIME PLOTS FOR TESTS NO. 30, 31, 21, 36, 37, AND 39

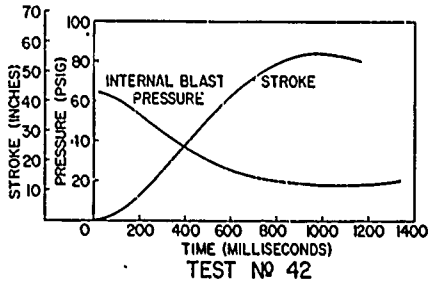

TEST № 42

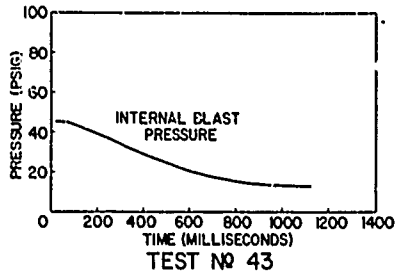

TEST № 43

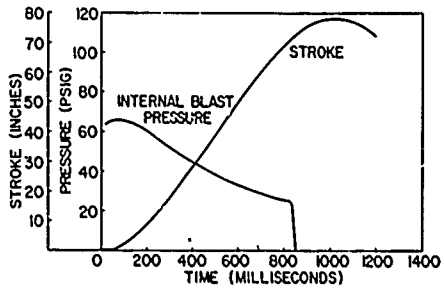

TEST № 41

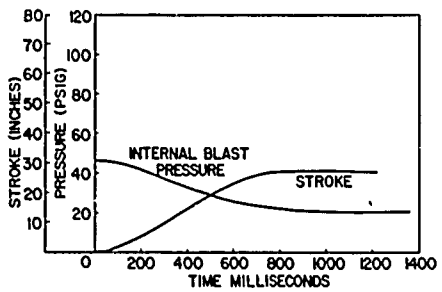

TEST № 44

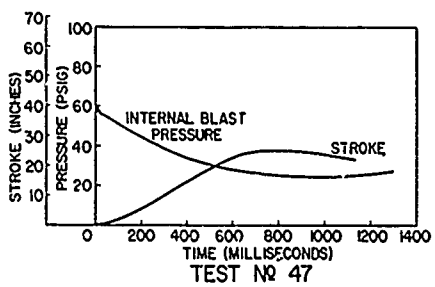

TEST № 47

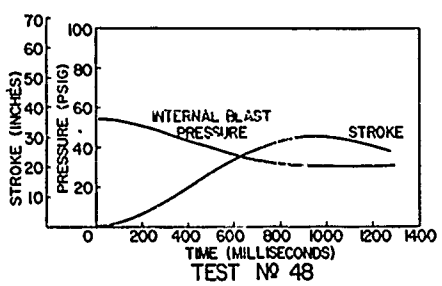

TEST № 48

FIG. 17 STROKE-TIME & PRESSURE-TIME PLOTS FOR TESTS NO. 42, 43, 41, 44, 47, AND 48

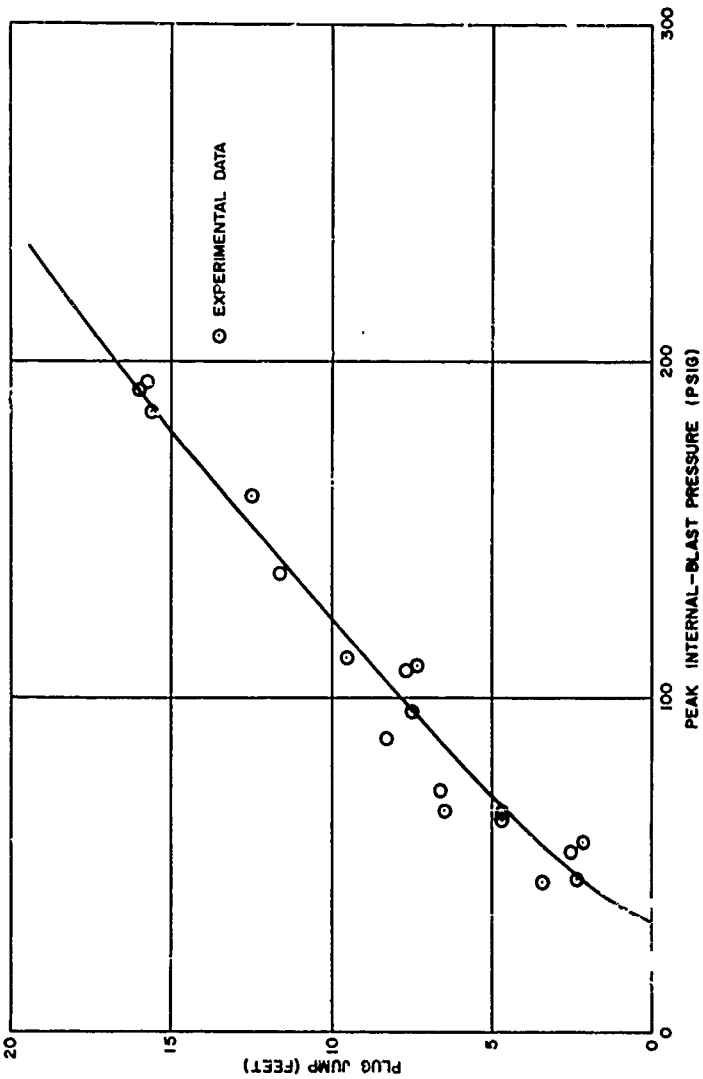

FIG.18 MODEL PLUG JUMP VS PEAK-PRESSURE CURVE

the data from the static-calibration records. The power stroke-time curves, also shown in the aforementioned figures, were obtained by coordinating the timing marks produced by the timing-pulse generator connected to the High-Speed Fairchild Camera with corresponding power stroke measurements. The power stroke-time plots, along with the maximum plug-jump data, were obtained from film read and analyzed on a Telereadex 29A film reader.

VALIDITY OF RESULTS

The over-all accuracy of the pressure-measuring system, including pressure gage, recorder, and data reduction, is believed to be within an error of ± 5% for the pressure data and ± 3% for the time data. The power stroke-time data are considered accurate to within ± 1% error for both stroke and time. The ± 1% error also holds true for the maximum plug-jump data obtained from the 35-millimeter Mitchell Camera records.

There is a fortunate element in the subject experiments, in that there is a technique available within each experiment by which confidence in the validity of the pressure-time data can be strengthened. This is accomplished essentially by utilizing the dynamics of the model plug in connection with the pressure-

time data to compare the energy available to move the plug with the maximum potential energy received by the plug. The analysis for increasing the confidence in the pressure-time data is as follows.

Assuming the system of forces acting upon the model plug as shown in the free-body diagram below

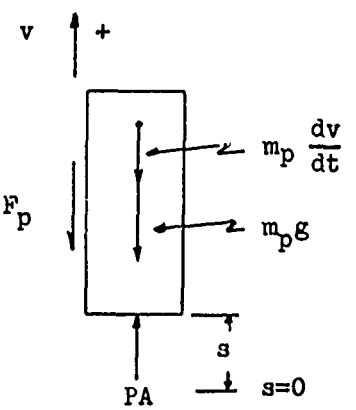

and neglecting wind losses, we find the equilibrium equation to be

$$PA = m_p \, v \, \frac{dv}{ds} + m_p \, g + F_p \qquad (16)$$

where the constants are

A .... frontal area of the plug, in^2

m_p ... mass of plug, slugs

g .... acceleration due to gravity, ft/sec^2

F_p ... frictional force, lb

and the variables are

P .... transient internal-blast pressure acting on frontal area, psig

v .... velocity of plug, ft/sec

s .... displacement of plug, ft.

The frictional force was measured at a slow constant velocity (about one in/sec) and was found to be approximately 20 pounds. Frictional-force measurements are discussed in Appendix B.

Rearranging equation (16) and integrating, we can write

$$A\int_{s=0}^{s=s_f} P\,ds = m_p\int_{v=0}^{v=v_f} v\,dv + m_p\,g\int_{s=0}^{s=s_f} ds + F_p\int_{s=0}^{s=s_t} ds \qquad (17)$$

where v_f and s_f are the velocity and the displacement of the plug, respectively, at the end of the power stroke and s_t is the displacement of the plug within the plug-guide tube. The values of s_f and s_t differed only in those tests where the maximum height achieved by the plug was greater than its power stroke. This difference is attributed to the fact that the length of the plug-guide tube was greater than the length of the pressure-sealed portion of the tube. Performing the indicated integration, we obtain

$$A \int_{s=0}^{s=s_f} P \, ds = \frac{m_p}{2} v_f^2 + m_p g s_f + F_p s_t \qquad (18)$$

One can utilize the maximum height achieved by the plug to determine its maximum increase in potential energy. From the conservation of energy, we can write

$$PE = m_p g H = \frac{m_p}{2} v_f^2 + m_p g s_f \qquad (19)$$

where

PE ... is maximum potential energy of plug, ft-lb

H .... is maximum height achieved by plug, ft.

Rearranging equation (19) and substituting into equation (18), we obtain

$$A \int_{s=0}^{s=s_f} P \, ds = F_p s_t + m_p g H \qquad (20)$$

which can be utilized to establish a confidence level for the pressure-time data. The value for $A \int_{s=0}^{s=s_f} P \, ds$ can be obtained by integrating the internal blast pressure-power stroke curve, which is developed by time synchronizing the internal blast pressure-time data with the power stroke-time data. The synchronization of the pressure-time curve with the power

stroke-time curve for Test No. 2 is shown in Figure 19. Integration of the pressure-power stroke curve was accomplished by measuring the area under the curve with a polar planimeter. Upon completion of the power stroke, pressure continued to act upon the frontal area of the plug for a short distance relative to the power stroke. That this effect is properly neglectable may be easily seen from the typical pressure-stroke curve shown in Figure 19. Knowing the weight ($m_p g$) and the maximum height achieved by the plug (H) as measured from the 35-millimeter Mitchell Camera records, we calculated the maximum potential energy. The energy lost to friction ($F_p\ s_t$) was calculated by assuming the measured frictional force of 20 pounds to be constant throughout the plug stroke. Let us define net pressure-force work to be gross pressure-force work less the energy lost to friction. Absolute percent deviations of net pressure-force work from maximum potential energy of the plug for the 21 tests are presented in Table 2. Internal blast pressure-power stroke plots developed by synchronization of the data presented in Figures 15, 16, and 17 are shown in Figures 20, 21, and 22.

For tests No. 36, 39, 42, 41, 47, and 48 in Table 2, the large percent deviation may be attributed to three factors: (1) the range of the pressure transducer used to measure the internal-blast pressure greatly exceeded the maximum pressure measured, thereby reducing its accuracy, (2) the energy lost

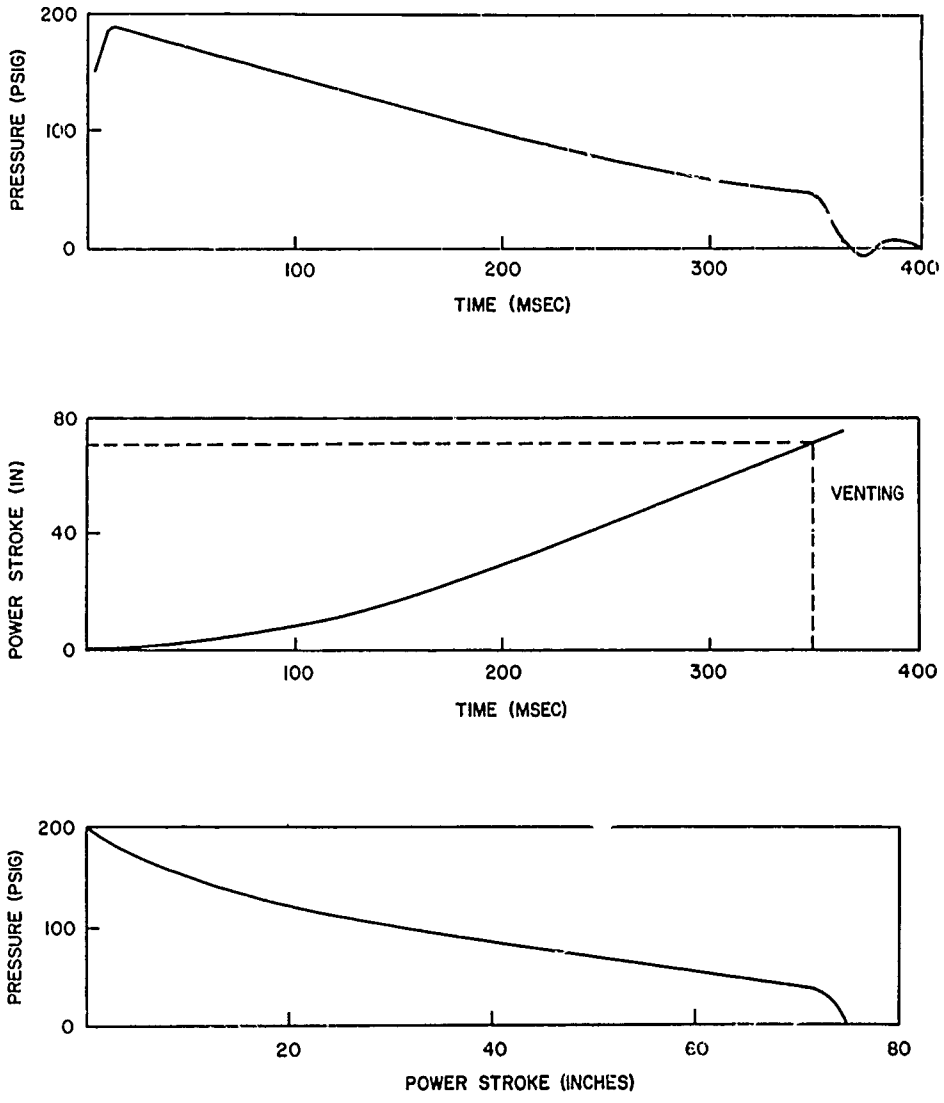

FIG. 19 TIME SYNCHRONIZATION OF PRESSURE-TIME & STROKE-TIME PLOTS FOR TEST NO. 2

TEST NO.	(1) $A\int P\,ds$	(2) $F_p s_t$	(3) $A\int P\,ds - F_p s_t$	(4) $m_p g H$	(5) COLUMN (3) - (4)	% DEVIATION $\frac{(5)}{(4)}$ 100
	(in-lbs)	(in-lbs)	(in-lbs)	(in-lbs)	(in-lbs)	(%)
2	63,264	1,929	61,335	58,438	2,897	4.96
29	62,113	1,929	60,184	57,669	2,515	4.36
35	60,227	1,929	58,298	57,194	1,104	1.93
23	36,829	1,929	34,900	34,712	188	0.54
25	29,150	1,929	27,221	26,693	528	1.98
24	33,000	1,929	31,071	28,304	2,767	9.78
30	47,951	1,929	46,022	45,806	216	0.47
31	46,450	1,929	44,521	42,511	2,010	4.73
21	30,383	1,929	28,454	27,755	699	2.52
36	21,974	1,140	20,834	17,246	3,588	20.80
37	31,749	1,929	29,820	30,428	608	2.00
38			MALFUNCTIONED PRESSURE GAGE			
39	28,805	1,547	27,231	24,020	3,211	13.37
40			MALFUNCTIONED PRESSURE GAGE			
42	19,992	1,120	18,872	16,990	1,882	11.08
43			MALFUNCTIONED HIGH-SPEED CAMERA			
41	29,171	1,564	27,607	23,873	3,734	15.64
44	9,082	550	8,532	8,422	110	1.31
45			MALFUNCTIONED PRESSURE GAGE			
47	9,390	497	8,893	7,579	1,314	17.34
48	12,440	600	11,840	9,154	2,686	29.34

TABLE 2 COMPARISON OF ENERGY AVAILABLE TO MOVE PLUG WITH MAXIMUM POTENTIAL ENERGY RECEIVED BY PLUG

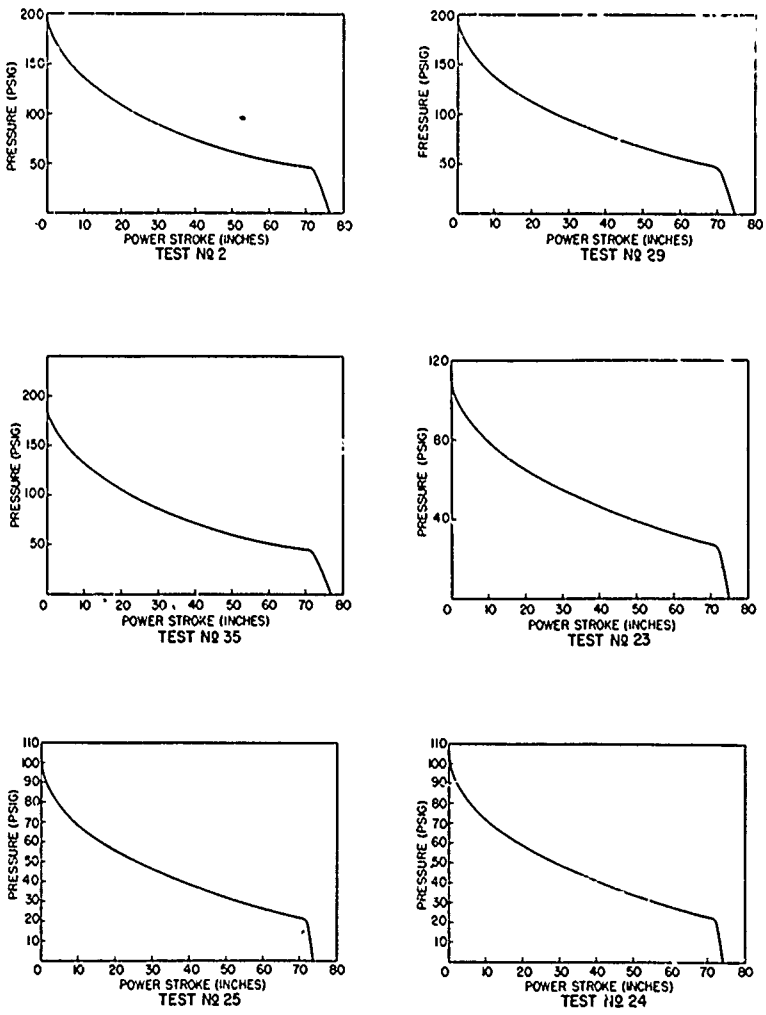

FIG 20 INTERNAL BLAST PRESSURE - POWER STROKE PLOTS FOR TESTS NO 2, 29, 35, 23, 25, AND 24

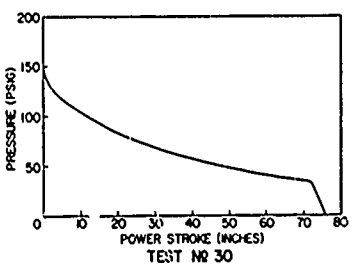

TEST NO 30

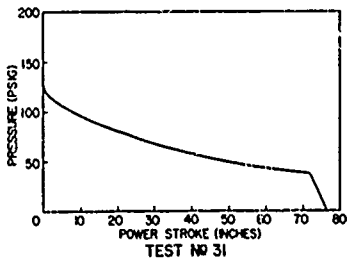

TEST NO 31

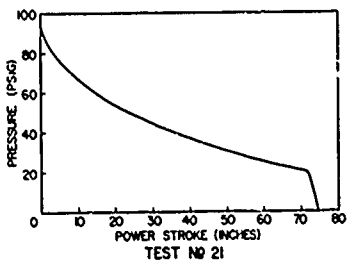

TEST NO 21

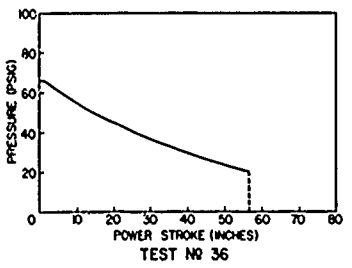

TEST NO 36

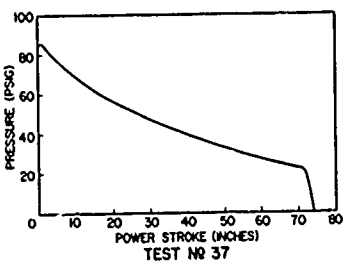

TEST NO 37

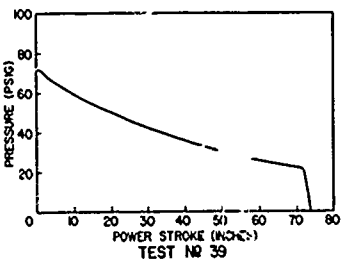

TEST NO 39

FIG. 21 INTERNAL BLAST PRESSURE-POWER STROKE PLOTS FOR TESTS NO. 30, 31, 21, 36, 37, AND 39

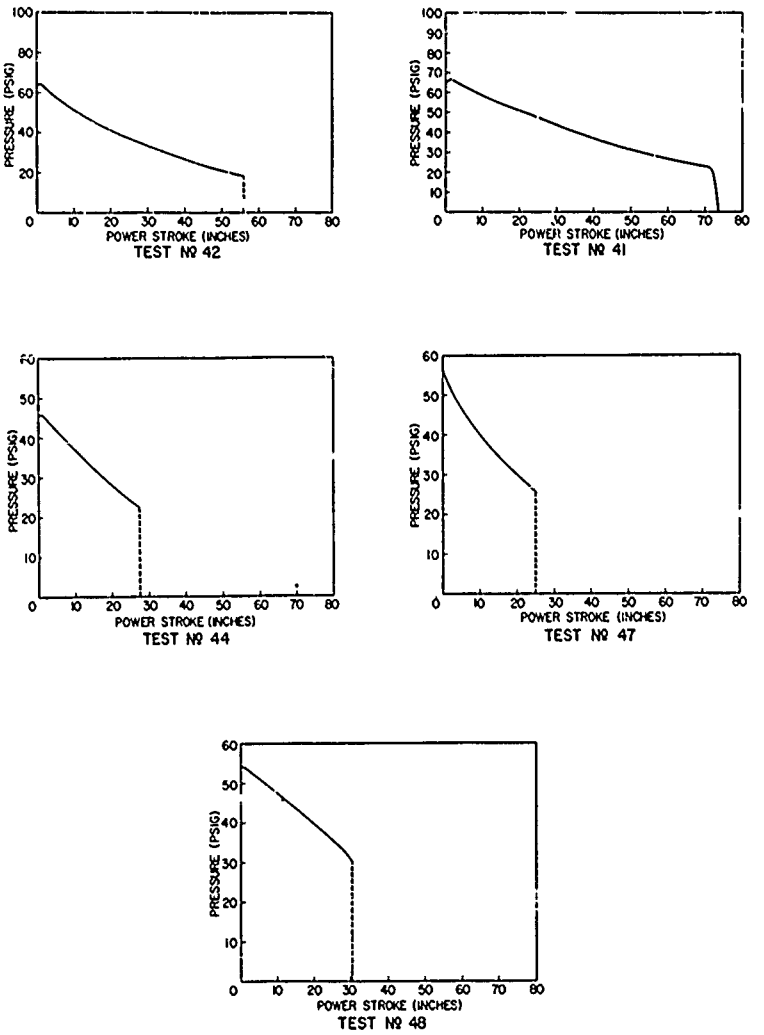

FIG 22 INTERNAL BLAST PRESSURE-POWER STROKE PLOTS FOR TESTS NO 42, 41, 44, 47 AND 48

due to friction was greater than that assumed, and (2) a shift between pre- and post-static calibration curves occurred.

SUMMARY AND CONCLUSIONS

The purpose of this study was to develop a method by which the internal blast pressure-time histories generated from the initiation of sodium-cased explosions surrounded by an oxygen-depleted atmosphere and confined within a closed piston-fitted vessel could be measured. A pressure-measuring system was developed, designed, fabricated, and employed to measure the internal blast pressure-time histories of 48 experiments conducted in a 1/30-scale idealized model reactor. In this report the pressure-time data for 21 of these experiments have been presented and evaluated for validity.

The pressure-measuring system essentially consisted of a recording oscilloscope and an electro-mechanical, variable-reluctance, diaphragm-type pressure gage coupled with a fluid-filled pressure-transmitting tube. The design of the pressure-transmitting tube was such that the response of the pressure gage could be controlled by varying the viscosity of the transmitting fluid. This control was essential in that it enabled the pressure gage to measure the internal-blast pressure with a reasonable degree of accuracy without being subjected to the damaging, high-pressure, shock pulse. The pressure-transmitting tube was proven effective, since pressure-time histories were

recorded wherein no explosive-shock pressures appeared and no damage of the pressure gage was experienced. Confidence in the validity of the pressure-time data recorded by the pressure-measuring system was strengthened by comparing the pressure-force work done on the model plug with the maximum potential energy received by the model plug.

The pressure-time histories, as recorded by the pressure-measuring instrumentation system, and presented herein, and the confidence in their validity affirm that this method for measuring the internal blast pressure-time histories of confined, sodium-cased explosions is a sound and workable one.

The author acknowledges a special debt of gratitude to Dr. Walter R. Wise, Jr., Research Mechanical Engineer, for his advice and guidance in directing the subject program and for his careful technical review of this presentation. The author is also indebted to Mr. Walter R. Anderson for his assistance in the design of the pressure-measuring instrumentation and for his help in measuring the internal blast pressure-time histories.

REFERENCES

(a) Fisher, E. M. and Wise, W. R., Jr. Containment Study of the Enrico Fermi Fast Breeder Reactor Plant. NAVORD Report 5747, 7 Oct 1957. Unclassified.

(b) Filler, W. S. Post-Detonation Pressure and Thermal Studies of Solid High Explosives in a Closed Chamber. NOL Reprint from Sixth Symposium (International) on Combustion.

(c) White, G. Liquid Filled Pressure Gage System. Statham Laboratories Instrument Note No. 7. Jan-Feb 1949.

(d) Timoshenko, S. Vibration Problems in Engineering. 3rd ed. New York: D. Van Nostrand Co. 1955.

APPENDIX A

DYNAMIC-CALIBRATION EXPERIMENTS

A series of dynamic-calibration experiments was conducted in order to evaluate the pressure-measuring instrumentation under transient pressure conditions. The objectives of the experiments were threefold: (1) to determine the dimensions of and the fluid viscosity within the pressure-transmitting tube necessary to produce the required damping, (2) to check out the complete pressure-measuring instrumentation prior to use in the model reactor experiments, and (3) to verify the damping theory. The assessed parameters in these experiments were main-section length and area, transmitting-fluid viscosity, and nozzle of the pressure-transmitting tube.

Recalling the schematic diagram of the pressure-sensing device from the section on Damping Theory, we have

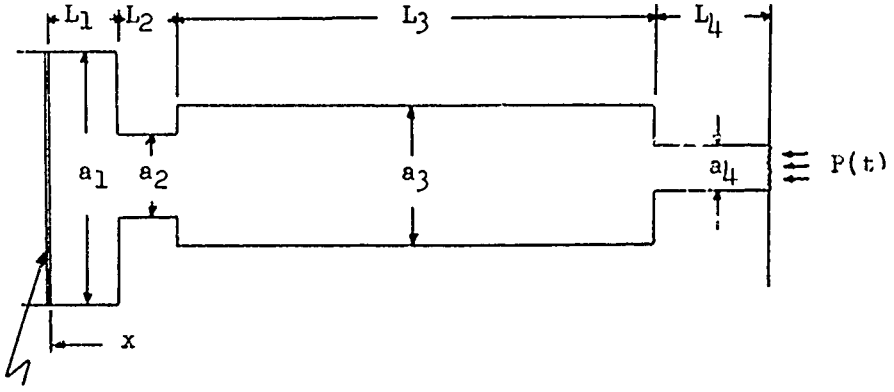

where subscripts denote

1 .... pressure-transducer section

2 .... pressure-transducer adapter section

3 .... transmitting-tube main section

4 .... transmitting-tube nozzle section.

The lengths and areas of the various tube sections investigated can be categorized into the following five cases:

Case 1 .... is pressure-sensing device <u>with</u> nozzle, where the dimensions are:

L_3 = 6.5 in; a_3 = 0.036 in^2

L_4 = 1.7 in; a_4 = 0.012 in^2

Case 2 .... is Case 1 <u>without</u> nozzle, where the dimensions are:

L_3 = 6.5 in; a_3 = 0.036 in^2

L_4 = 0.0 in; a_4 = 0.000 in^2

Case 3 .... is Case 1 with <u>length of main section shortened</u>, where the dimensions are:

L_3 = 2.5 in; a_3 = 0.036 in^2

L_4 = 1.7 in; a_4 = 0.012 in^2

Case 4 .... is Case 3 <u>without</u> nozzle, where the dimensions are:

L_3 = 2.5 in; a_3 = 0.036 in^2

L_4 = 0.0 in; a_4 = 0.000 in^2

Case 5 .... is Case 4 with <u>inside diameter of main section enlarged</u>, where the dimensions are:

L_3 = 2.5 in; a_3 = 0.111 in^2

L_4 = 0.0 in; a_4 = 0.000 in^2

The dimensions for tube sections 1 and 2 are common to all five cases and are as follows:

$L_1 = 0.16$ in; $a_1 = 0.197$ in^2

$L_2 = 1.00$ in; $a_2 = 0.023$ in^2

Ten tests were performed in which the pressure-sensing devices defined by the aforementioned five cases were filled with 200- and 2,000-centistoke, "200" Dow Corning Corporation silicone fluid and subjected to transient pressure pulses of 100-psig magnitude and of the order of 500-microseconds rise time. These pressure pulses were generated in a pressure pot, a cross-sectional view of which is shown in Figure 14. A chronological description of the procedure in performing dynamic-calibration tests is as follows. The pressure-sensing device was filled under a vacuum with the silicone fluid being investigated and inserted securely into the gage chamber of the pressure pot. The gage chamber was sealed from the reference chamber with the sealing valve. The inertia spring and mass were cocked and retained by the tripping trigger to which the inertial starter was attached. The inertial starter was then raised and held in position with the lanyard pin. The reference chamber was filled to the pressure at which the sensing device was to be calibrated by air supplied from compressed air bottles. When the desired pressure within the reference chamber, measured by the chamber-pressure gage, was reached, the lanyard pin was pulled, triggering the cocked inertia spring and mass. The inertia mass, in turn,

abruptly released the sealing valve, subjecting the pressure-sensing device in the gage chamber to a sharp-rising pressure pulse. The motion of the inertia mass, prior to its unsealing the sealing valve, also closed a microswitch causing a trigger pulse to be delivered to the recording oscilloscope. A view of the dynamic-calibration setup is shown in Figure A-1.

The oscilloscope traces for these ten tests are shown in Figures A-2 and A-3. The pressure-sensing device was filled with 200-centistoke silicone oil in those tests presented in Figure A-2, whereas 2,000-centistoke silicone fluid was used in those presented in Figure A-3. In making a comparison of the experimental results with theory for the degree of damping of the system, one must recall the expression for the degree of damping

$$h = \frac{r_t}{r_c} \tag{9}$$

where

$$r_t = 8\pi\mu\left[L_1 + \frac{a_1}{a_2} L_2 + \frac{a_1}{a_3} L_3 + \frac{a_1}{a_4} L_4\right]$$

$$r_c = 2\sqrt{k\, m_t} \tag{10}$$

If we recall equation (14)

$$m_t = m_d + \frac{4}{3}\rho\left\{a_1 L_1 + a_2 L_2 \left[\frac{a_1}{a_2}\right]^2 + a_3 L_3 \left[\frac{a_1}{a_3}\right]^2 + a_4 L_4 \left[\frac{a_1}{a_4}\right]^2\right\} \tag{14}$$

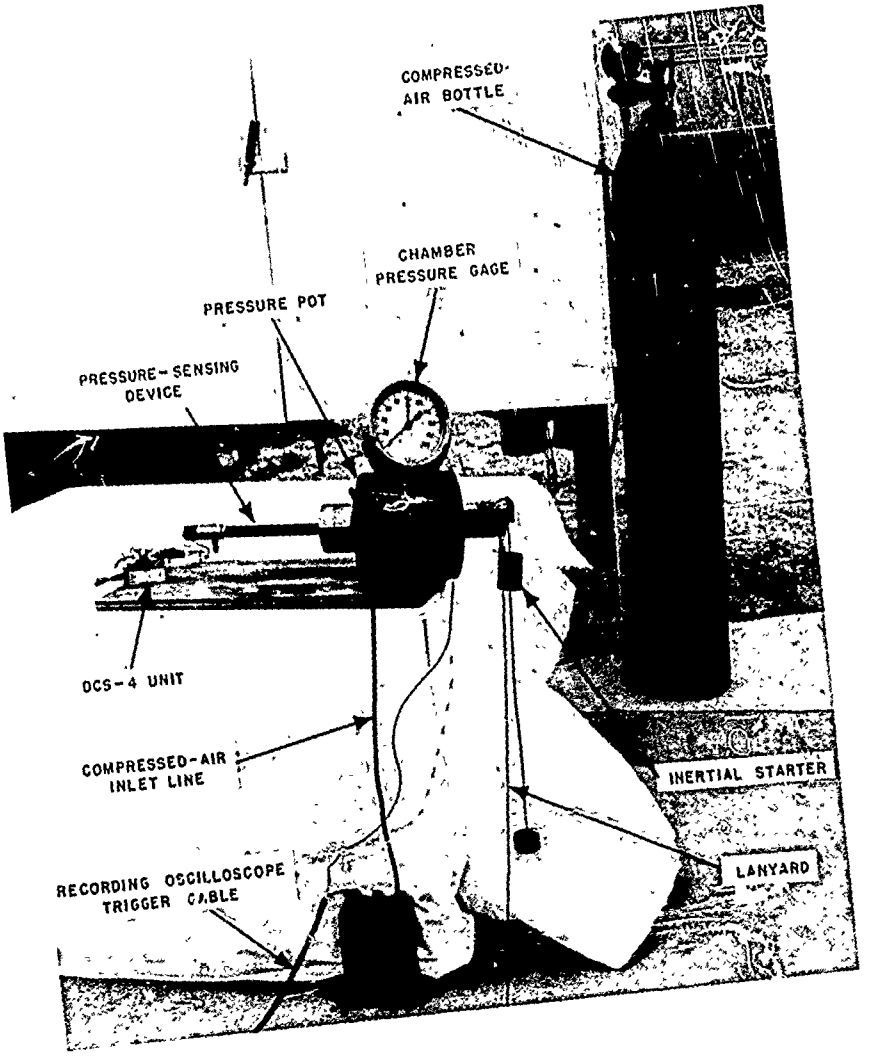

FIG. A-1 DYNAMIC CALIBRATION SETUP

CASE 1

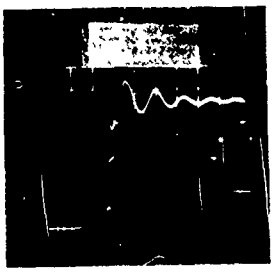

PRESSURE-SENSING DEVICE *WITH* NOZZLE

CASE 2

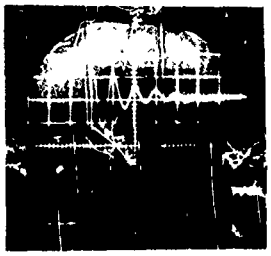

CASE 1 *WITHOUT* NOZZLE

CASE 3

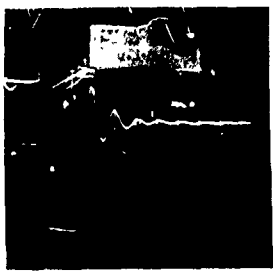

CASE 1 WITH *LENGTH* OF MAIN SECTION *SHORTENED*

CASE 4

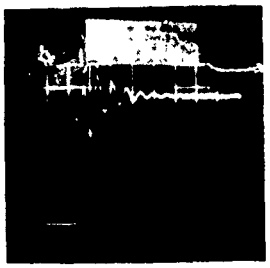

CASE 3 *WITHOUT* NOZZLE

CASE 5

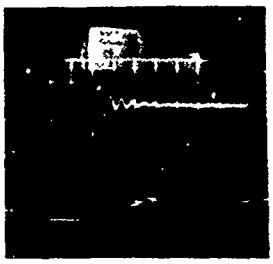

CASE 4 WITH *INSIDE DIAMETER* OF MAIN SECTION *ENLARGED*

NOTES: ALL CASES WERE SUBJECTED TO 100-PSI PULSE.

TIME BASE FOR ALL TESTS WAS 2 MSEC / CM

FIG. A-2 OSCILLOSCOPE TRACES SHOWING DEGREES OF DAMPING OF 100-PSI GAGE FILLED WITH 200-CENTISTOKE SILICONE OIL

CASE 1

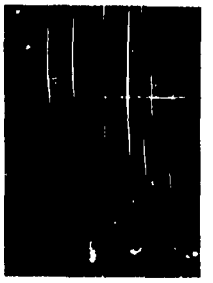

PRESSURE-SENSING DEVICE *WITH* NOZZLE

CASE 3

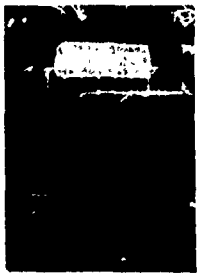

CASE 1 WITH *LENGTH* OF MAIN SECTION *SHORTENED*

CASE 4

1 CM

CASE 3 *WITHOUT* NOZZLE

CASE 5

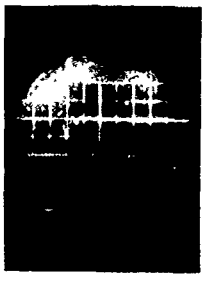

CASE 4 WITH *INSIDE DIAMETER* OF MAIN SECTION *ENLARGED*

NOTE: ALL CASES WERE SUBJECTED TO 100-PSI PULSE.
TIME BASE FOR ALL TESTS WAS 2 MSEC/CM.

FIG. A-3 OSCILLOSCOPE TRACES SHOWING DEGREES OF DAMPING OF 100-PSI GAGE FILLED WITH 2000-CENTISTOKE SILICONE OIL

the degree of damping can also be expressed as

$$h = \frac{4\pi\mu\left[L_1 + \frac{a_1}{a_2} L_2 + \frac{a_1}{a_3} L_3 + \frac{a_1}{a_4} L_4\right]}{\sqrt{k\, m_t}} \qquad (15a)$$

The value for the spring constant, k, of the diaphragm can be determined from its load deflection relationship, which is

$$k = \frac{P\, a_1}{\delta} \qquad (21)$$

where

δ .... is deflection of the diaphragm.

The expression for δ can be obtained by considering the diaphragm to be a uniformly loaded, circular plate with clamped edges under large deflection. This is a good assumption in that the diaphrag. is mounted in such a manner as to fulfill the clamped-edges condition and the maximum deflection of the diaphragm does not exceed that of its thickness. The expression for δ is obtained from Reference (d), and is

$$\delta = \frac{P\, d_1^4}{1024\, D} \quad \frac{1}{1 + .488\, \frac{\delta^2}{w^2}} \qquad (22)$$

where

d .... is diameter of diaphragm, i.

w .... is thickness of diaphragm, in

D .... is flexural rigidity of diaphragm, lb-in

and

$$D = \frac{E\, w^3}{12\,(1 - \nu^2)} \tag{23}$$

where

E .... is modulus of elasticity in tension and compression of diaphragm, lb/in^2

ν .... is Poisson's ratio of diaphragm.

Results calculated from the Damping Theory and measured from the experimental data for the ten experiments performed are presented in Table A-1. For the purpose of comparing the measured experimental results with the theoretical calculated results, it is more meaningful to express the degree of damping in terms of the natural damped frequency, f_{nd}, of the system, since this is more readily measured. From equation (8) the natural damped frequency of the system can be expressed as

$$f_{nd} = \frac{1}{2\pi}\sqrt{\frac{k}{m_t} - \left[\frac{r_t}{2m_t}\right]^2} \tag{24}$$

The conclusions that can be drawn from the results presented in Table A-1 are as follows:

1. The experimental results qualitatively affirm the damping theory.

CASE TYPE	200-CENTISTOKE DAMPING FLUID			2000-CENTISTOKE DAMPING FLUID		
	r_t/r_c	f_{nd}		r_t/r_c	f_{nd}	
	CALCULATED	CALCULATED	MEASURED	CALCULATED	CALCULATED	MEASURED
		CPS	CPS		CPS	CPS
1	9.75×10^{-2}	239	358	9.75×10^{-1}	38	0
2	4.62×10^{-2}	293	500	4.62×10^{-1}	220	*
3	9.73×10^{-2}	275	417	9.73×10^{-1}	48	0
4	3.66×10^{-2}	420	750	3.66×10^{-1}	341	715
5	2.62×10^{-2}	550	900	2.62×10^{-1}	478	900

*. No data obtained for this test

TABLE A-I DYNAMIC-CALIBRATION EXPERIMENTAL RESULTS, MEASURED AND CALCULATED

2. An increase in the viscosity of the transmitting fluid decreases the natural damped frequency and increases the damping of the system. This is shown by comparing the tests that used 200-centistoke damping fluid with the tests that used 2000-centistoke damping fluid. The effect that viscosity of fluid has upon the damping is less as the damping of the system is reduced. This is shown by Cases 4 and 5.

3. A decrease in the length of the main section of the pressure-transmitting tube increases the natural damped frequency and decreases the damping. This is shown by comparing, for the tests that used 200-centistoke fluid, Cases 1 and 2 with Cases 3 and 4, respectively. For the tests that used 2000-centistoke fluid, Cases 1 and 3 were overdamped, resulting in a non-oscillatory condition. By comparing the rise time of the pressure pulse for Cases 1 and 3 shown in Figure A-3, the effect of the length of the main section upon the damping can be shown.

4. An increase in the diameter of the main section of the transmitting tube increases the natural damped frequency and decreases the damping. This is shown by comparing Case 4 with Case 5.

5. The addition of the nozzle decreases the natural damped frequency and increases the damping. This is shown by comparing Cases 1 and 3 with Cases 2 and 4, respectively. In the tests that used 2000-centistoke fluid, the effect of the

nozzle can be shown in Figure A-3 by comparing the rise time of the pressure pulse of Case 1 with that of Case 3.

From the results obtained in these tests, a transmitting tube of the Case 1 design, filled with 2000-centistoke silicone fluid, was used in the model reactor experiments. Additional tests were performed in order to investigate the damping characteristic of Case 1 type transmitting tube under a wider range of transmitting-fluid viscosities. The oscilloscope traces for these tests are presented in Figure A-4.

A similar series of experiments conducted with the fluid-damping type pressure-transmitting tube was also conducted with the orifice-damping type transmitting tube. The results of these tests revealed that the required damping characteristic was produced by a 1/8-inch diameter orifice.

Sample Calculations. Sample calculations for Case 1 (transmitting tube filled with 200-centistoke silicone fluid) are presented here.

The dimensions and physical properties for Case 1 are as follows:

$$L_1 = 0.16 \text{ in}; \qquad a_1 = 0.197 \text{ in}^2$$
$$L_2 = 1.00 \text{ in}; \qquad a_2 = 0.023 \text{ in}^2$$
$$L_3 = 6.50 \text{ in}; \qquad a_3 = 0.036 \text{ in}^2$$
$$L_4 = 1.70 \text{ in}; \qquad a_4 = 0.012 \text{ in}^2$$

$$\mu = 200 \text{ (centistoke)} \times 1.4095 \times 10^{-7} = 2.819 \times 10^{-5} \frac{\text{lb-sec}}{\text{in}^2}$$

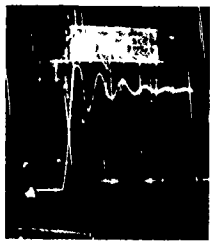

200-CENTISTOKE SILICONE OIL
100-PSI PULSE
TIME: 2 MSEC/CM

1000-CENTISTOKE SILICONE OIL
100-PSI PULSE
TIME: 2 MSEC/CM

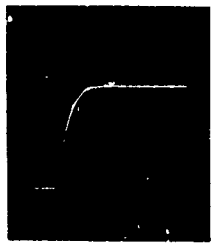

2000-CENTISTOKE SILICONE OIL
100-PSI PULSE
TIME: 2 MSEC/CM

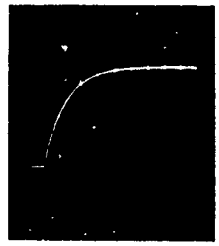

12,500 CENTISTOKE SILICONE OIL
100-PSI PULSE
TIME: 5 MSEC/CM

NOTE: ALL TESTS WERE CONDUCTED WITH 7-INCH TRANSMITTING TUBE WITH NOZZLE (CASE I)

FIG. A-4 OSCILLOSCOPE TRACES SHOWING EFFECT OF VARYING OIL VISCOSITY IN PRESSURE-TRANSMITTING TUBE

Dimensions of 100-psi pressure-transducer diaphragm are

$$w = 0.008 \text{ in}$$

$$d = 0.500 \text{ in}$$

$$\nu = 0.28$$

$$D = 1.005 \text{ lb-in}$$

$$m_d g = 4.57 \times 10^{-4} \text{ lb}$$

From equation (22)

$$\delta = \frac{(100)\ (0.500)^4}{(1024)\ (1.005)} \times \frac{1}{1 + 0.488\ \frac{\delta^2}{(0.008)^2}}$$

the solution of which gives

$$\delta = 0.005 \text{ in}$$

and upon substituting in equation (21), we calculate k to be

$$k = \frac{(100)\ (0.197)}{(0.005)} = 3880 \text{ lb/in}$$

From equation (14) we calculate m_t to be

$$m_t = 4.57\times10^{-4} + \frac{4}{3}\ (3.515\times10^{-2})\ \left[\ (0.197)(0.16) + (0.023)(1)\left(\frac{0.197}{0.023}\right)^2 + (0.036)(6.50)\left(\frac{0.197}{0.036}\right)^2 + (0.012)(1.70)\left(\frac{0.197}{0.012}\right)^2\ \right]$$

$$= 1.69\times10^{-3} \text{ slugs}$$

From the calculated values for k and m_t, h from equation (15a) becomes

$$h = \frac{4\pi\, 2.819\text{x}10^{-5}\left[0.16 + \frac{0.197}{0.023}(1) + \frac{0.197}{0.036}(6.50) + \frac{0.197}{0.012}(1.70)\right]}{\sqrt{(3880)(1.69\text{x}10^{-3})}}$$

$$= 9.75\text{x}10^{-2}$$

Combining equations (9), (10), and (15a), we obtain

$$r_t = 9.75\text{x}10^{-2}\,(2)\,\sqrt{(3880)(1.69\text{x}10^{-3})} = 0.499 \text{ lb-sec/in}$$

Then from equation (24) f_{nd} becomes

$$f_{nd} = \frac{1}{2\pi}\sqrt{\frac{3880}{1.69\text{x}10^{-3}} - \left(\frac{0.499}{2 \text{ x } 1.69\text{x}10^{-3}}\right)^2} = 239 \text{ cps.}$$

APPENDIX B

FRICTIONAL-FORCE MEASUREMENTS

In order to establish confidence in the validity of the pressure-time data, it was necessary to have some idea as to the magnitude of the frictional force of the model plug. A system was devised in which a Dillon Force Gage was utilized in measuring the frictional force of the plug. A setup of this system is illustrated in Figure B-1. The force gage was calibrated under known loads, then placed in series with the plug, steel rod, steel ball, and hydraulic lift. The plug was then raised at a slow uniform rate by the lift through an approximate stroke of four feet, and the force measured by the gage was noted. After the plug had reached the top of its stroke, it was lowered to its initial position, and once again the force measured by the gage was noted. This procedure was repeated several times, and the average readings of the force required to raise and lower the plug were taken. The frictional force was then determined from the following relationship

$$\frac{\text{Force (up)} - \text{Force (down)}}{2} = \text{Frictional Force} \qquad (25)$$

and it was checked by using the following expression

$$\text{Force (up)} - \text{Plug weight} = \text{Frictional Force} \qquad (26)$$

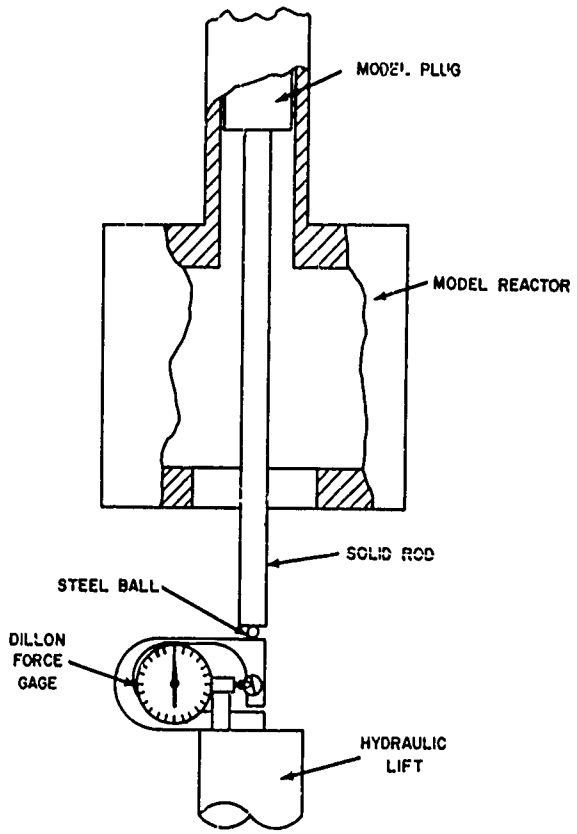

FIG. B-1 FRICTIONAL-FORCE MEASURING SETUP

A constant frictional force of 20 pounds was determined from this series of tests, the accuracy of which is of the order of ± 5 pounds. This accuracy was such that no difference could be distinguished between static friction and the kinetic friction.

DISTRIBUTION

	Copies
National Bureau of Standards Room 301 Northwest Building Washington 25, D. C. Attn: Library	1
National Bureau of Standards Washington 25, D. C. Attn: Dr. C. Muehlhause	1
Chief of Naval Operations, D/N Code 418 Washington 25, D. C.	1
Chief of Naval Research, D/N Bldg. T-3 Washington 25, D. C.	2
Director, U. S. Naval Research Laboratory Washington 25, D. C.	1
Director, Office of Naval Research Branch Office, 1000 Geary Street San Francisco, California	1
Chief, Bureau of Naval Weapons Washington 25, D. C. Attn: Library, DIS 3	2
Chief, Bureau of Naval Weapons Washington 25, D. C. Attn: (RRRE) W. T. August	1
Bureau of Naval Weapons Department of the Navy Code RMMO-13 Washington 25, D. C. Attn: Mr. Edward M. Fisher	1
Commanding Officer U. S. Naval Weapons Evaluation Facility Kirtland AFB, Albuquerque, New Mexico	1
Commander, Naval Weapons Laboratory Dahlgren, Virginia	1
Chief, Bureau of Ships Department of the Navy Washington 25, D. C.	1

DISTRIBUTION

	Copies
Atomic Energy Commission Washington 25, D. C. Attn: Technical Library	3
Atomic Power Development Associates, Inc. Nuclear and Analytic Division 1911 First Street, Detroit 26, Michigan Attn: Mr. Walter J. McCarthy, Jr. Dr. Alton Klickman	2
Atomics International P.O. Box 309, Canoga Park, California Attn: Mr. A. A. Jarrett Mr. J. W. Flora	2
Babcock and Wilcox Company Atomic Energy Division 161 East 42nd Street New York 17, New York Attn: M. A. Cordovi	1
Ballistic Research Laboratories Aberdeen Proving Ground, Maryland Attn: Mr. Orlando T. Johnson	1
Brookhaven National Laboratory Technical Information Division Upton, Long Island, New York Attn: Research Library	2
University of California Institute of Engineering Research Berkeley 4, California Attn: Dr. Virgil E. Schrock Mr. H. A. Johnson	2
University of California Lawrence Radiation Laboratory Technical Information Division P.O. Box 808, Livermore, California	2
Carnegie Institute of Technology Schenley Park, Pittsburgh 19, Pennsylvania Attn: Dr. Emerson M. Pugh	1
Combustion Engineering, Inc. Reactor Development Division Union Street, Windsor, Connecticut Attn: Francis Bonacci	1

DISTRIBUTION

	Copies
Advisory Committee on Reactor Safeguards Room H-1147, Matomic Building 1717 H Street, N. W., Washington 25, D. C. Attn: Dr. T. J. Thompson Dr. D. Duffey Mr. J. B. Graham Mr. R. F. Fraley	4
Allied Chemical & Dye Corporation General Chemical Division 40 Rector Street, New York 6, N. Y. Attn: Mr. K. R. Osborn, Manager Industrial Development	1
Allied Chemical & Dye Corporation Morristown, New Jersey Attn: Mr. D. A. Rogers, Manager Central Engineering	1
Allis Chalmers Manufacturing Company Nuclear Power Department, Box 512 Milwaukee 1, Wisconsin Attn: Mr. C. B. Graham	1
Argonne National Laboratory 9700 So. Cass Avenue, Argonne, Illinois Attn: Dr. R. C. Vogel	2
Chief, Defense Atomic Support Agency The Pentagon, Washington 25, D. C.	2
Armed Services Technical Information Agency Arlington Hall Station, Arlington 12, Virginia	10
Armour Research Foundation 10 West 35th Street, Chicago 16, Illinois Attn: Dr. T. A. Zaker Dr. N. A. Weil	2
Atomic Energy Commission Army Reactors, Division of Reactor Development Washington 25, D. C.	1
Chicago Operations Office, U. S. Atomic Energy Commission 9800 So. Cass Avenue, Argonne, Illinois Attn: Mr. D. Gardiner	1

DISTRIBUTION

	Copies
Commanding Officer and Director David Taylor Model Basin Washington 7, D. C.	1
Director of Defense Research and Engineering The Pentagon Washington 25, D. C.	1
Duke University Department of Physics Durham, North Carolina Attn: Dr. H. W. Newson	1
E. I. duPont de Nemours and Company Explosives Department Atomic Energy Division Wilmington 98, Delaware Attn: Document Custodian	1
Chief of Engineers Department of the Army Washington 25, D. C. Attn: ENGEB	1
Frankford Arsenal Bridge and Tacony Streets Philadelphia 37, Pennsylvania Attn: Librarian	1
General Electric Company Atomic Power Equipment Department 2155 South Street San Jose, California Attn: Library	1
General Nuclear Engineering Corporation P.O. Box 245 Dunedin, Florida	1
Harvard University School of Public Health 55 Shattuck Street Boston 15, Massachusetts Attn: Dr. Leslie Silverman	1

DISTRIBUTION

	Copies
Harvard University Cambridge, Massachusetts Attn: Dr. Harvey Brooks Dean of Engineering and Applied Physics	1
Hercules Powder Company Research Department Wilmington, Delaware Attn: Dr. Willard P. Conner, Manager Physical Chemical Division	1
Internuclear Company 7 North Brentwood Boulevard Clayton 5, Missouri	1
Director, Applied Physics Laboratory Johns Hopkins University Baltimore 18, Maryland	1
Research Analysis Corporation 6935 Arlington Road Washington 14, D. C. Attn: Document Control Office	1
Johns Hopkins University Department of Sanitary Engineering and Water Resources Baltimore 18, Maryland Attn: Mr. John C. Geyer	1
Knolls Atomic Power Laboratory P. O. Box 1072, Schenectady, New York Attn: Document Librarian	2
Liberty Mutual Insurance Company 175 Berkeley Street Boston 17, Massachusetts Attn: Dr. C. R. Williams	1
Los Alamos Scientific Laboratory P. O. Box 1663, Los Alamos, New Mexico Attn: Report Librarian	2
Mound Laboratory Monsanto Chemical Company P. O. Box 32, Miamisburg, Ohio	1

DISTRIBUTION

	Copies
Nuclear Development Corporation of America 5 New Street White Plains, New York Attn: Library	1
Oak Ridge Institute of Nuclear Studies P.O. Box 117 Oak Ridge, Tennessee Attn: Library	1
Oak Ridge National Laboratory P.O. Box X Oak Ridge, Tennessee Attn: Mr. William Cottrell Mr. Frank Bruce Dr. W. K. Ergen Dr. F. A. Gifford, Jr. Dr. F. C. Maienschein	5
Pacific Missile Range Code 4113, P.O. Box 10 Point Mugu, California Attn: Mr. Harry B. Benefiel	2
U. S. Patent Office Scientific Library Washington 25, D. C.	1
Phillips Petroleum Company Manager, Reactor Projects P.O. Box 1259 Idaho Falls, Idaho Attn: Mr. Warren E. Nyer	1
U. S. Pipe and Foundry Company Steel and Tubes Division Burlington, New Jersey Attn: Dr. A. E. Schuh	1
Commanding Officer Picatinny Arsenal Dover, New Jersey	1
Sandia Corporation Sandia Base, Albuquerque, New Mexico Attn: Library	1

DISTRIBUTION

	Copies
Space Technology Laboratories, Inc. P.O. Box 1085, Los Angeles 45, California Attn: Dr. D. B. Langmuir Mr. Sam Zivi	2
Stanford Research Institute Poulter Laboratory Menlo Park, California Attn: Dr. Donald Davenport Mr. Neilan B. Botsford	2
The Travelers Insurance Companies 700 Main Street, Hartford 15, Connecticut Attn: Mr. Reul C. Stratton, Asst. Director Department of Research	1
Office of Technical Services U. S. Department of Commerce Washington 25, D. C.	4
Technical Information Service Extension U. S. Atomic Energy Commission P.O. Box 62, Oak Ridge, Tennessee	5
Union Carbide Nuclear Company P.O. Box 1223, Paducah, Kentucky Attn: Library	1
Vitro Engineering Division Technical Reports Section 225 Fourth Avenue, New York 3, New York	1
Commanding Officer, Watertown Arsenal Watertown 72, Massachusetts Attn: Technical Information Section	1
Westinghouse Electric Corporation Commercial Atomic Power Activity P.O. Box 355, Pittsburgh 30, Pennsylvania Attn: Document Custodian	1
Atomic Energy Commission Maritime Reactors Branch Division of Reactor Development Washington 25, D. C.	1

DISTRIBUTION

	Copies
Atomic Energy Commission Civilian Reactors, Division of Reactor Development Washington 25, D. C. Attn: Mr. D. H. Stewart	1
Atomic Energy Commission Assistant Director for Reactors Division of Compliance Washington 25, D. C.	1
Director, Division of Research U. S. Atomic Energy Commission Washington 25, D. C.	1
Atomic Energy Commission Hazards Evaluations Branch Division of Licensing and Regulation Washington 25, D. C. Attn: Mr. Edson Case	7
Idaho Operations Office U. S. Atomic Energy Commission P.O. Box 1221, Idaho Falls, Idaho Attn: Mr. J. B. Philipson	1
Atomic Energy Commission Naval Reactors Branch Division of Reactor Development Washington 25, D. C. Attn: Mr. T. Rockwell Mr. R. S. Brodsky	2
Atomic Energy Commission Radiation Branch, Environmental Sciences Division New York Operations Office 376 Hudson Street, New York 14, N. Y. Attn: Mr. James E. McLaughlin	1
Atomic Energy Commission Research and Development Branch Division of Reactor Development Washington 25, D. C. Attn: Mr. S. A. Szawlewicz	2
San Francisco Operations Office U. S. Atomic Energy Commission 2111 Bancroft Way, Berkeley 4, California Attn: Mr. G. H. Helfrich	1

DISTRIBUTION

	Copies
Atomic Energy Commission Canoga Park Area Office P. O. Box 591 Canoga Park, California Attn: Mr. C. W. Richards	1
Atomic Energy Commission Idaho Operations Office P. O. Box 2108 Idaho Falls, Idaho Attn: Mr. G. E. Devore Mr. D. William	2
USAEC Technical Representative Toronto, Ontario Canada Attn: Mr. D. Glenn Boyer	1
Brookhaven National Laboratory Upton, New York Attn: Mr. A. W. Castlemann	1
University of Minnesota Department of Chemical Engineering Minneapolis, Minnesota Attn: Prof. H. Isbin	1
Phillips Petroleum Company P. O. Box 1259 Idaho Falls, Idaho Attn: Mr. Frank Schroeder Mr. Glenn O. Bright Mr. T. R. Wilson	7

CATALOGING INFORMATION FOR LIBRARY USE

BIBLIOGRAPHIC INFORMATION

	DESCRIPTORS	CODES		DESCRIPTORS	CODES
SOURCE	NOL technical report	NOLTR	SECURITY CLASSIFICATION AND CODE COUNT	Unclassified - 25	UØ25
REPORT NUMBER	62-45	62ØØ45	CIRCULATION LIMITATION		
REPORT DATE	9 August 1962	Ø862	CIRCULATION LIMITATION OR BIBLIOGRAPHIC		
			BIBLIOGRAPHIC (SUPPL., VOL., ETC.)		

SUBJECT ANALYSIS OF REPORT

DESCRIPTORS	CODES	DESCRIPTORS	CODES	DESCRIPTORS	CODES
Blast	BLAS	Plug	PLUG	Gage	GAGE
Pressure	PRES	Reactor	REAC		
Confined	CTAI	Nuclear	NUCL		
Explosions	EXPS	Simulation	SIMU		
Measurement	MEAU	Excursion	EXCU		
Internal	INTO	Explosive	EXPL		
Time	TIME	Charges	CHAR		
Sodium	SODI	Loadings	LOAI		
Cased	CASE	Response	RESP		
Models	MODE	Oscilloscope	OSCS		
Fermi	FRMI	Electric	ELEC		
Shield	SHIL	Mechanical	MECA		

PRNC-NOL-5070/28 (5-62)

Naval Ordnance Laboratory, White Oak, Md.
(NOL technical report 62-45)
A METHOD FOR MEASURING INTERNAL BLAST PRESSURE-TIME HISTORIES OF CONFINED, SODIUM-CASED EXPLOSIONS (U), by Harry B. Benefiel. 9 Aug. 1962. v.p. Task NOL-285 UNCLASSIFIED

Experiments in models were conducted to assess response of the Enrico Fermi shield plug to explosively simulated nuclear excursions. Internal blast pressures generated by sodium-cased explosive charges were measured with a variable reluctance gage coupled with a transmission tube that responds to the internal blast pressure but not to the shock. Pressure data from some of these experiments, a description of the complete pressure-instrumentation system, and an analysis of the damping characteristics of the transmission tube are presented in considerable detail.

1. Reactors - Enrico Fermi
2. Explosions - Blast
3. Explosions - Measurements
4. Pressure measurements
5. Pressure systems

I. Title
II. Benefiel, Harry B.
III. Project

Abstract card is unclassified.

Naval Ordnance Laboratory, White Oak, Md.
(NOL technical report 62-45)
A METHOD FOR MEASURING INTERNAL BLAST PRESSURE-TIME HISTORIES OF CONFINED, SODIUM-CASED EXPLOSIONS (U), by Harry B. Benefiel. 9 Aug. 1962. v.p. Task NOL-285 UNCLASSIFIED

Experiments in models were conducted to assess response of the Enrico Fermi shield plug to explosively simulated nuclear excursions. Internal blast pressures generated by sodium-cased explosive charges were measured with a variable reluctance gage coupled with a transmission tube that responds to the internal blast pressure but not to the shock. Pressure data from some of these experiments, a description of the complete pressure-instrumentation system, and an analysis of the damping characteristics of the transmission tube are presented in considerable detail.

1. Reactors - Enrico Fermi
2. Explosions - Blast
3. Explosions - Measurements
4. Pressure measurements
5. Pressure systems

I. Title
II. Benefiel, Harry B.
III. Project

Abstract card is unclassified.

Naval Ordnance Laboratory, White Oak, Md.
(NOL technical report 62-45)
A METHOD FOR MEASURING INTERNAL BLAST PRESSURE-TIME HISTORIES OF CONFINED, SODIUM-CASED EXPLOSIONS (U), by Harry B. Benefiel. 9 Aug. 1962. v.p. Task NOL-285 UNCLASSIFIED

Experiments in models were conducted to assess response of the Enrico Fermi shield plug to explosively simulated nuclear excursions. Internal blast pressures generated by sodium-cased explosive charges were measured with a variable reluctance gage coupled with a transmission tube that responds to the internal blast pressure but not to the shock. Pressure data from some of these experiments, a description of the complete pressure-instrumentation system, and an analysis of the damping characteristics of the transmission tube are presented in considerable detail.

1. Reactors - Enrico Fermi
2. Explosions - Blast
3. Explosions - Measurements
4. Pressure measurements
5. Pressure systems

I. Title
II. Benefiel, Harry B.
III. Project

Abstract card is unclassified.

Naval Ordnance Laboratory, White Oak, Md.
(NOL technical report 62-45)
A METHOD FOR MEASURING INTERNAL BLAST PRESSURE-TIME HISTORIES OF CONFINED, SODIUM-CASED EXPLOSIONS (U), by Harry B. Benefiel. 9 Aug. 1962. v.p. Task NOL-285 UNCLASSIFIED

Experiments in models were conducted to assess response of the Enrico Fermi shield plug to explosively simulated nuclear excursions. Internal blast pressures generated by sodium-cased explosive charges were measured with a variable reluctance gage coupled with a transmission tube that responds to the internal blast pressure but not to the shock. Pressure data from some of these experiments, a description of the complete pressure-instrumentation system, and an analysis of the damping characteristics of the transmission tube are presented in considerable detail.

1. Reactors - Enrico Fermi
2. Explosions - Blast
3. Explosions - Measurements
4. Pressure measurements
5. Pressure systems

I. Title
II. Benefiel, Harry B.
III. Project

Abstract card is unclassified.